# Towards a satellite formaldehyde – in situ hybrid estimate for organic aerosol abundance

Jin Liao[1,2], Thomas F. Hanisco[1], Glenn M. Wolfe[1,3], Jason St. Clair[1,3], Jose L. Jimenez[4,5], Pedro Campuzano-Jost[4,5], Benjamin A. Nault[4,5], Alan Fried[6], Eloise A. Marais[7,*], Gonzalo Gonzalez Abad[8], Kelly Chance[8], Hiren T. Jethva[1,2], Thomas B. Ryerson[9], Carsten Warneke[9,5], Armin Wisthaler[10,11]

[1]Atmospheric Chemistry and Dynamic Laboratory, NASA Goddard Space Flight Center, Greenbelt, MD, USA
[2]Universities Space Research Association, GESTAR, Columbia, MD, USA
[3]University of Maryland Baltimore County, Joint Center for Earth Systems Technology, Baltimore, MD, USA
[4]Department of Chemistry, University of Colorado, Boulder, Colorado, USA
[5]Cooperative Institute for Research in the Environmental Sciences, University of Colorado, Boulder, Colorado, USA
[6]Department of Atmospheric and Oceanic Sciences, University of Colorado Boulder, Boulder, Colorado, USA
[7]School of Geography, Earth and Environmental Sciences, University of Birmingham, UK
[8]Harvard-Smithsonian Center for Astrophysics, Cambridge, Massachusetts, USA
[9]NOAA Earth System Research Laboratory (ESRL), Chemical Sciences Division, Boulder, CO, USA
[10]Department of Chemistry, University of Oslo, Oslo, Norway
[11]Institute for Ion Physics and Applied Physics, University of Innsbruck, Innsbruck, Austria
[*]now at Department of Physics and Astronomy, University of Leicester, Leicester, UK

Correspondence email: jin.liao@nasa.gov

**Abstract**

Organic aerosol (OA) is one of the main components of the global particulate burden and intimately links natural and anthropogenic emissions with air quality and climate. It is challenging to accurately represent OA in global models. Direct quantification of global OA abundance is not possible with current remote sensing technology; however, it may be possible to exploit correlations of OA with remotely observable quantities to infer OA spatiotemporal distributions. In particular, formaldehyde (HCHO) and OA share common sources via both primary emissions and secondary production from oxidation of volatile organic compounds (VOCs). Here, we examine OA-HCHO correlations using data from summer time airborne campaigns investigating biogenic (NASA SEAC$^4$RS and DC3), biomass burning (NASA SEAC$^4$RS) and anthropogenic conditions (NOAA CalNex and NASA KORUS-AQ). In situ OA correlates well with HCHO ($r = 0.59 - 0.97$), and the slope and intercept of this relationship depend on the chemical regime. For biogenic and anthropogenic regions, the OA-HCHO slopes are higher in low $NO_x$ conditions, because HCHO yields are lower and aerosol yields are likely higher. The OA-HCHO slope of wild fires is over 9 times higher than that for biogenic and anthropogenic sources. The OA-HCHO slope is higher for highly polluted anthropogenic sources (e.g., KORUS-AQ) than less polluted (e.g., CalNex) anthropogenic sources. Near-surface OA over the continental US are estimated by combining the observed in situ relationships with HCHO column retrievals from NASA's Ozone Monitoring Instrument (OMI). HCHO vertical profiles used in OA estimates are from climatology a-priori profiles in the OMI HCHO retrieval or output of specific period from a newer version of GEOS-Chem. Our OA estimates compare well with US EPA IMPROVE data obtained over summer months

(e.g., slope = 0.60-0.62, r = 0.56 for August 2013), with correlation performance comparable to intensively validated GEOS-Chem (e.g., slope = 0.57, r = 0.56) with IMPROVE OA and superior to the satellite-derived total aerosol extinction (r = 0.41) with IMPROVE OA. This indicates that OA estimates are not very sensitive to these HCHO vertical profiles and that a priori profiles from OMI HCHO retrieval have a similar performance to that from the newer model version in estimating OA. Improving the detection limit of satellite HCHO and expanding in situ airborne HCHO and OA coverage in future missions will improve the quality and spatiotemporal coverage of our OA estimates, potentially enabling constraints on global OA distribution.

## 1. Introduction

Aerosols are the largest source of uncertainty in climate radiative forcing (IPCC 2013; Carslaw et al., 2013) and decrease atmospheric visibility and impact human health (Pope 2002). Organic aerosols (OA) comprise a large portion (~50%) of submicron aerosols (Jimenez et al., 2009; Murphy et al., 2006; Shrivastava et al., 2017), and this fraction will grow with continued decline in $SO_2$ emissions (Attwood et al., 2014; Marais et al., 2017; Ridley et al., 2018). In addition, OA serve as cloud condensation nuclei (CCN) and affect cloud formation and climate radiative forcing. OA components also have adverse health effects (e.g., Walgraeve et al., 2010) and contribute significantly to regional severe haze events (e.g., Hayes et al., 2013). Finally, because the response of temperature to changes in climate forcing is non-linear (Taylor and Penner, 1994) and the forcing by aerosols has strong regional character (Kiehl and Briegleb, 1993), it is necessary to separate out different climate forcing components to accurately forecast the climate response to changes in forcing.

Despite their importance, it has been challenging to accurately represent OA in global models. Chemical transport models (CTMs) often under-predict OA (e.g., more than a factor of 2 lower OA near the ground) compared to observations, and model-to-model variability can exceed a factor of 100 in the free troposphere (Tsigaridis et al., 2014; Heald et al., 2008; Heald et al., 2011). Fully explicit mechanisms have attempted to capture the full OA chemical formation mechanisms (e.g., Lee-Taylor et al., 2015), but it is too computationally expensive to apply these mechanisms to OA formation in global CTMs at a useful resolution. For computational efficiency, 3-D models such as GEOS-

87 Chem include direct emissions of primary OA (POA) and represent secondary OA (SOA)
88 formation either by lumping SOA products according to similar hydrocarbon classes
89 (Kim et al., 2015) or based on the volatility of the oxidation products (Pye et al., 2010).
90 Marais et al. (2016) applied an aqueous phase mechanism for SOA formation from
91 isoprene in GEOS-Chem to reasonably simulate isoprene SOA in the southeastern (SE)
92 US. Schroder et al. (2018) showed GEOS-Chem has a very large under prediction of
93 SOA in the Northeastern US dominated by anthropogenic emissions. Accurate emission
94 inventories are also needed to correctly represent volatile organic compounds (VOCs)
95 and $NO_x$ ($NO_x$ = NO + $NO_2$) inputs, and these often have biases compared to
96 observational constraints (Kaiser et al., 2018, Travis et al., 2016, Anderson et al., 2014;
97 McDonald et al., 2018).
98
99 A quantitative measure of OA from space would be helpful for verifying emissions and
100 aerosol processes in models. However, direct measurements of OA from space are
101 currently unavailable. Aerosol optical depth (AOD) measured by satellite sensors
102 provides a coarse but global picture of total aerosol distributions. Multi-angle Imaging
103 SpectroRadiometer (MISR) provides aerosol property information such as size, shape and
104 absorbing properties, which allows retrieving the AOD of a subset of aerosols (Kahn and
105 Gaitley, 2015). Classification algorithms have been developed to speciate different
106 aerosol types (e.g., OA) based on AOD, extinction Angstrom exponent, UV Aerosol
107 Index, and trace gas columns from satellite instruments (de Vries et al., 2015). Here we
108 aim to provide a quantitative estimation of OA mass concentrations from satellite
109 measurements.

Formaldehyde (HCHO) is one of the few VOCs that can be directly observed from space. Sources emitting POA (e.g., biomass burning (BB)) often simultaneously release VOCs. HCHO and SOA are also both produced from emitted VOCs. VOCs, as well as intermediate- and semi- volatile organic compounds (I/SVOCs), are oxidized by hydroxyl radicals (OH) to form peroxy radicals ($RO_2$), which then react with NO, $RO_2$, or hydroperoxy radicals ($HO_2$) or isomerize. These oxidation processes produce HCHO and oxidized organic compounds with low volatility that condense to form SOA (Robinson et al., 2013; Ziemann and Atkinson, 2012). The yield of HCHO and SOA from hydrocarbon oxidation thus depends on the VOC precursors, oxidants (OH, $O_3$ and $NO_3$), $RO_2$ reaction pathway (e.g., NO levels), and pre-existing aerosol abundance and properties (Wolfe et al., 2016; Pye et al., 2010; Marais et al., 2016 and 2017; Xu et al., 2016). Moreover, although the lifetime of HCHO (1-3 hrs) is shorter than OA (1 week), HCHO continues to form from slower reacting VOCs, as well as from the oxidation of later generation products. Observations across megacities around the world show that OA formation in polluted/urban area happens over about 1 day (e.g., DeCarlo et al., 2010; Hodzic and Jimenez, 2011; Hayes et al., 2013; 2015), and HCHO is also significantly formed over this timescale (Nault et al., 2018). In addition, Veefkind et al. (2011) found that satellite AOD correlated with HCHO over the summer time SE US, BB regions, and Southeast Asian industrialized regions. This also suggests that OA share common emission sources and photochemical processes with HCHO and are a major contributor to AOD in the regions above. Marais et al. (2016) further used the relationship between aircraft OA and

satellite HCHO to evaluate GEOS-Chem representation of SOA mass yields from biogenic isoprene in the SE US.

We present an OA surface mass concentration estimate (OA estimate) derived from a combination of satellite HCHO column observations and in situ OA-HCHO relationships. Because the detection limit of satellite HCHO column observations limit the quality of OA estimate, we focus our analyses on summer time when HCHO levels are high. The OA estimate is evaluated against OA measurements at ground sites. A 3-D model GEOS-Chem OA simulation is shown for comparison.

## 2. Methods

### 2.1 In situ airborne observations

Figure 1 shows flight tracks with altitudes < 1 km of the field campaigns used in the current study. The Studies of Emissions, Atmospheric Composition, Clouds and Climate Coupling by Regional Surveys (SEAC$^4$RS) mission (Toon et al., 2016) covered the continental US with a focus on the SE US in August-September 2013. The Deep Convective Clouds & Chemistry Experiment (DC3) (Barth et al., 2015) surveyed the central and SE US in May-June 2012, targeting isolated deep convective thunderstorms and mesoscale convective systems. The California Research at the Nexus of Air Quality and Climate Change (CalNex) (Ryerson et al., 2013) investigated the California region in May-June 2010, targeting the Los Angeles (LA) Basin and Central Valley. The Korea-United States Air Quality Study (KORUS-AQ) studied South Korean air quality, sampling many large urban areas in South Korea and continental Asian outflow over the

West Sea, in May-June 2016 (Aknan and Chen, 2017). KORUS-AQ only includes data with longitude < 133° E to exclude the transit from US because it targeted South Korea and the nearby region. These field campaigns were selected as they had recent high-quality in situ HCHO and OA data measured with state-of-the-art instruments and studied summer time regional tropospheric chemical composition.

In situ airborne HCHO observations were acquired by multiple instruments. The DC3 NASA DC-8 payloads featured two HCHO measurements: the NASA In Situ Airborne Formaldehyde (ISAF) (Cazorla et al., 2015) and the Difference Frequency Generation Absorption Spectrometer (DFGAS) (Weibring et al., 2006). The SEAC$^4$RS NASA DC-8 payloads also featured two HCHO measurements: the NASA ISAF and the Compact Atmospheric Multispecies Spectrometer (CAMS) (Richter et al., 2015). HCHO measurements from ISAF were found to be in good agreement with CAMS, with a correlation coefficient of 0.99 and a slope of 1.10 (Zhu et al., 2016). HCHO measurements from ISAF also had a good agreement with DFGAS, with a correlation coefficient of 0.98 and a slope of 1.07. Because ISAF has higher data density, we used ISAF HCHO data for DC3 and SEAC$^4$RS. During KORUS-AQ, CAMS was the only HCHO instrument onboard the DC-8. In CalNex a proton transfer reaction mass spectrometer (PTR-MS) (Warneke et al., 2011) was used to measure HCHO on board the NOAA P3 aircraft.

In situ airborne OA from SEAC$^4$RS, DC3, and KORUS-AQ was measured by the University of Colorado High-Resolution Time-of-Flight Aerosol Mass Spectrometer

178 (AMS, DeCarlo et al., 2006; Dunlea et al., 2009; Canagaratna et al., 2007; Jimenez et al.,
179 2016) and in situ airborne OA from CalNex was measured by the NOAA Compact Time-
180 of-Flight Aerosol Mass Spectrometer (Drewnick et al., 2005; Canagaratna et al., 2007;
181 Bahreini et al., 2012). The OA measurements are from 1 min merge data and converted
182 from μg $sm^{-3}$ (at 273 K and 1013 mbar) to μg $m^{-3}$ under local T & P for each data point,
183 to be consistent with HCHO concentrations in μg $m^{-3}$ or molec $cm^{-3}$ at local T & P.
184
185 Although NO modulates the $RO_2$ lifetime, and thus, the production of HCHO and SOA,
186 NO cannot be directly observed via remote sensing. Instead, $NO_2$ can be directly
187 observed in space by satellites, and because $NO_2$ represents typically ~80% (e.g.,
188 SEAC$^4$RS and KORUS-AQ) of the boundary layer $NO_x$ concentrations during the
189 daytime, $NO_2$ can be used as a surrogate for daytime NO concentrations and oxidative
190 conditions around the globe. In situ airborne $NO_2$ was measured by the NOAA
191 Chemiluminescence $NO_yO_3$ instrument (Ryerson et al., 2001) during SEAC$^4$RS and by
192 University of Berkeley laser induced fluorescence $NO_2$ instrument (Day et al., 2002)
193 during KORUS-AQ. SEAC$^4$RS isoprene measurements were from proton-transfer-
194 reaction mass spectrometer (PTR-MS) (Wisthaler et al., 2002).
195
196 **2.2 Ground-based OA measurements**
197 Ground-based OA measurements over the US were from the EPA Interagency
198 Monitoring of Protected Visual Environments (IMPROVE) (Malm et al., 1994; Solomon
199 et al., 2014; Hand et al., 2014; Hand et al., 2013; Malm et al., 2017) and Southeastern
200 Aerosol Research and Characterization (SEARCH) (Edgerton et al., 2006) networks. In

201 the IMPROVE network, aerosols were collected on quartz fiber filters and analyzed in
202 the lab by thermal optical reflectance for organic and elemental carbon. The data were
203 reported every three days from 1988 to 2014. Monthly averages were used for
204 comparison in this study. IMPROVE OA data over the SE US (east of 70ºW) in summer
205 time were multiplied by a factor of 1.37 to correct for partial evaporation during filter
206 transport, following the recommendation of a comparison study with SEARCH organic
207 carbon (OC) measurements (Kim et al., 2015; Hand et al., 2013). Although IMPROVE
208 OA corrected for evaporation has potential uncertainties with the constant scaling factor,
209 the IMPROVE measurements have high spatial coverage. SEARCH network (Edgerton
210 et al., 2006; Hidy et al., 2014) OC was determined by the difference between total carbon
211 (TC) detected by a tapered element oscillating microbalance (TEOM) and black carbon
212 (BC) measured by an in situ Thermal Optical instrument. This allowed real-time
213 measurement of OC and prevented evaporation during filter transport. Although the
214 SEARCH network only has 5 sites available, we used observations from this network due
215 to their high accuracy. The IMPROVE and SEARCH network OC measurements were
216 converted to OA by multiplying by a factor of 2.1 based on ground and aircraft
217 observations (Pye et al., 2017; Schroder et al., 2018).
218
219 **2.3 Satellite measurements**
220 Satellite HCHO column observations were derived from the NASA's Ozone Monitoring
221 Instrument (OMI), a UV/Vis nadir solar backscatter spectrometer on the Aura satellite
222 (Levelt et al., 2006). Aura overpasses the equator at 1:30 pm local time, daily. Here we
223 used the OMI HCHO version 2.0 (collection 3) gridded (0.25°× 0.25°) retrieval data

(Gonzalez Abad et al., 2015) from the Smithsonian Astrophysical Observatory (SAO). Satellite data for HCHO columns were subjected to data quality filters: 1) solar zenith angle lower than 70°, 2) cloud fraction less than 40%, and 3) main quality flag and the xtrackquality flag both equal to zero (Harvard-Smithsonia Center for Astrophysics OMI HCHO data product description). The monthly average HCHO columns were also weighted by the column uncertainties of the pixels. The HCHO retrieval used a priori profiles without aerosol information from the GEOS-Chem model (Gonzalez Abad et al., 2015). Satellite $NO_2$ column observations were also derived from NASA's OMI level 3 data (Lamsal et al., 2014; NASA OMI $NO_2$ data archive). Satellite $NO_2$ observations were used to calculate $NO_x$ related chemical factor dependent OA estimate (see Table 2). Satellite AOD observations were acquired from the Moderate Resolution Imaging Spectroradiometer (MODIS) onboard the Aqua satellite, using overpasses at about 1:30 pm local time. Here, we used collection 06 (NASA MODIS AOD data archive), retrieved using the Dark Target (DT) and Deep Blue (DB) algorithms (Levy et al., 2015), monthly average data.

### 2.4 GEOS-Chem

We used GEOS-Chem (v9-02) at 2° × 2.5° with 47 vertical layers to simulate HCHO and OA globally, the same as that in Marais et al. (2016). GEOS-Chem was driven with meteorological fields from the NASA Global Modeling and Assimilation Office (GMAO). The OA simulation included POA from fires and anthropogenic activity and SOA from the volatility-based reversible partitioning scheme (VBS) of Pye et al. (2010) for anthropogenic, fire, and monoterpene sources, and an irreversible aqueous-phase

247 reactive uptake mechanism for isoprene. The aqueous-phase mechanism was coupled to
248 gas-phase isoprene chemistry and has been extensively validated using surface and
249 aircraft observations of isoprene SOA components in the SE US (Marais et al., 2016).
250 This model version used the fourth-generation global fire emissions database (GFED4)
251 (Giglio et al., 2013) as BB emission inventory. The model was driven with Goddard
252 Earth Observing System – Forward Processing (GEOS-FP) meteorology for 2013 and
253 sampled along the SEAC$^4$RS (2013) and KORUS-AQ (2016) flight tracks. The model
254 was also run with 10% decrease in biomass burning, biogenic, or anthropogenic
255 emissions as a sensitivity test to evaluate the contributions of different sources to OA and
256 HCHO budget. Model monthly mean surface layer OA and total column formaldehyde
257 were obtained around the OMI overpass time (12:00-15:00 local time) for 2008-2013
258 using Modern-Era Retrospective analysis for Research and Applications (MERRA)
259 (Gelaro et al., 2017) meteorology, as GEOS-FP was only available from 2012. This was
260 compared to the OA estimate derived from satellite HCHO.
261
262 Global isoprene emissions from the Model of Emissions of Gases and Aerosols from
263 Nature version 2.1 (MEGAN) (Guenther et al., 2006) and satellite $NO_2$ column data were
264 used to calculate an isoprene and $NO_2$ dependent OA estimate (see Table 2). Global
265 isoprene emissions from MEGAN were implemented in GEOS-Chem and driven with
266 MERRA (MEGAN-MERRA).
267

268 **2.5 Estimation of surface organic aerosol mass concentrations**

An estimate for surface OA mass concentration was calculated based on a simple linear transformation.

$$\varepsilon(\mathrm{i}) = \Omega_{HCHO}(\mathrm{i})\eta(\mathrm{i})\alpha(i) + \beta(\mathrm{i}) \quad \text{Eq. (1)}$$

Here, $\varepsilon$(i) is the OA estimate for grid cell i (μg $m^{-3}$), $\Omega_{HCHO}$(i) is the OMI HCHO column density (molec $cm^{-2}$) in each 0.25° × 0.25° grid cell (similar resolution to OMI HCHO nadir pixel data), $\eta$(i) is the ratio of midday surface layer (~60 m) HCHO concentrations (molec $cm^{-3}$) to column concentrations (molec $cm^{-2}$) from GEOS-Chem, and $\alpha(i)$ and $\beta$(i) are the slope and intercept of a linear regression between OA and HCHO from low altitude (<1 km) airborne in situ measurements. The in situ to column conversion factor $\eta$(i) was similar to that used by Zhu et al. (2017) to convert HCHO columns into surface concentrations. $\eta$(i) was derived from the HCHO a priori profiles used in SAO OMI air mass factor (AMF) calculations (GEOS-Chem v9-01-03 climatology) or from GEOS-Chem v9-02, which included updated isoprene scheme for OA and is the next version of the model (v9-01-03) for a priori profiles used in SAO satellite HCHO retrievals. HCHO a priori profiles were used to be consistent with satellite HCHO retrievals and also to show that OA estimate can be derived without running a global model separately. The newer version of GEOS-Chem was used to test the sensitivity of OA estimates to updated version of $\eta$. The newer version of GEOS-Chem also allows sampling through the flight tracks of a recent field campaign (SEAC$^4$RS) and examining the factors impacting $\eta$ with both modeled and measured HCHO profiles. The detailed information about the impact of HCHO profiles on $\eta$ is provided in Sect. 5.

**2.6 Aerosol extinction from satellite measurements**

Currently remote sensing techniques observe aerosols by quantifying AOD. The MISR satellite instrument can estimate a subset of AOD, using constraints on size range, shape and absorbing properties, but it cannot distinguish OA from other submicron aerosol compounds such as sulfate and nitrate and also requires AOD to be above 0.1. Because MISR estimates a subset of AOD, it is discussed above to verify that we are not neglecting a satellite dataset that has already captured OA AOD. Moreover, OA account for a large and relatively constant fraction of submicron aerosols in the SE US (Kim et al., 2015; Wagner et al., 2015) and are one of the major submicron aerosol components over the US (Jimenez et al., 2009). Therefore, AOD was converted to extinction to represent OA for comparison.

$$A_{ext} = \mathrm{AOD(i)}\delta\mathrm{(i)} \qquad \text{Eq. (2)}$$

where $A_{ext}$ is the calculated aerosol extinction ($Mm^{-1}$), AOD(i) is aerosol optical depth from MODIS (see Sect. 2.3) in each 0.25°×0.25° grid cell, and $\delta$(i) ($m^{-1}$) is the ratio of surface layer OA concentrations ($\mu g\ m^{-3}$, at ambient T & P) to column OA concentrations ($\mu g\ m^{-2}$) from GEOS-Chem multiplied by $10^6$ $Mm^{-1}/m^{-1}$ . The shape of the average vertical profile of OA (OA fraction: 0.54-0.7) was close to that of total aerosol mass over SE US (Wagner et al., 2015) where a large fraction of the enhanced non-BB aerosol concentrations in summer time over the US are located. Data with BB plumes interferences were excluded in the following analysis. The potential contribution of dust and nitrate could alter the shape of the vertical profiles and introduce uncertainties when using OA vertical profiles for other parts of the US. However, the outliners in the aerosol extinction compared to ground OA measurements (see Sec. 6.3) were not located outside of the SE US. Similar vertical profile shapes of OA and submicron particles were also

observed in a campaign outside the US over South Korea (Nault et al., 2018). Although OA accounted for ~40% of the total submicron particles, the shape of OA and total submicron particles vertical profiles were nearly identical.

## 3. In situ OA-HCHO relationship

Although OA and HCHO share common VOC emission sources and photochemical processes, their production rates from different emission sources and photochemical conditions vary, as do their loss rates. We found the main factors that modulate OA-HCHO relationships from in situ measurements and discussed in the following section.

### 3.1 Regional and Source-Driven Variability

For all regions and/or sources investigated, near-surface in situ OA and HCHO are well correlated. A scatter plot of in situ OA vs. HCHO at low altitudes (<1 km) from a number of field campaigns (SEAC$^4$RS, DC3, CalNex, and KORUS-AQ) is displayed in Fig. 2. The slopes, intercepts, and correlation coefficients are summarized in Table 1. SEAC$^4$RS, DC3, and CalNex excluded BB data when acetonitrile > 200 pptv (Hudson et al., 2004). KORUS-AQ used a BB filter with higher acetonitrile (>500 pptv) because the air masses with moderate acetonitrile enhancement (200-500 pptv) were actually from anthropogenic emissions. This attribution is based on high levels of acetonitrile detected downwind of Seoul and west coastal petrochemical facilities, the slope between acetonitrile and CO being to urban emissions (Warneke et al., 2006), and the concentrations of anthropogenic tracer $CHCl_3$ being high (Warneke et al., 2006). Similar to acetonitrile, another common BB tracer hydrogen cyanide (HCN) was also enhanced

338 in these air masses. BB data (acetonitrile > 200 pptv) for SEAC$^4$RS were analyzed
339 separately and are inset in Fig. 2. Although all CalNex data had a tight correlation, we
340 only included the flight data near LA basin to target the area strongly influenced by
341 anthropogenic emissions. In general, the correlation coefficients between in situ OA and
342 HCHO were strong (r = 0.59 –0.97) (Table 1).
343
344 The variety in OA-HCHO regression coefficients among different campaigns reflects the
345 regional and/or source-driven OA-HCHO variability. Considering only the non-biomass
346 burning (non-BB) air masses sampled, OA and HCHO had the tightest correlation for
347 CalNex, because CalNex focused on the LA area (shown in Fig. 2) and Central Valley
348 while SEAC$^4$RS and DC3 covered a larger area with a potentially larger variety of
349 sources and chemical conditions. Although SEAC$^4$RS and DC3 both sampled the
350 continental US, SEAC$^4$RS had more spatial coverage and sampled more air masses at low
351 altitudes, while DC3 was designed to sample convective outflow air masses and had more
352 data at high altitudes. Although KORUS-AQ covered a much smaller area compared to
353 SEAC$^4$RS, KORUS-AQ data also had a large spread, which may be due to the
354 complicated South Korean anthropogenic sources mixed with transported air masses
355 (e.g., from China) and maybe biogenic sources. OA exhibits a tight correlation with
356 HCHO for both wildfires and agricultural fires during SEAC$^4$RS. This is because the
357 production of HCHO and OA is much higher in BB air masses compared to background.
358 This may also suggest that the emissions of OA and HCHO in these air masses are
359 relatively constant. SEAC$^4$RS data are chosen because it sampled fires and had state-of-
360 the-art, high quality measurements. More intensive fire sampling is needed to probe the
361 correlation between OA and HCHO across fuel types and environmental conditions.

The different slopes of OA-HCHO among different campaigns also reflect the regional or source-driven OA-HCHO variability. Among the BB, anthropogenic and biogenic sources, the slopes of OA vs. HCHO for BB air masses were the highest. This is consistent with high POA emission in BB conditions (Heald et al., 2008; Lamarque et al., 2010; Cubison et al., 2011), with low addition of mass due to SOA formation (Cubison et al., 2011; Shrivastava et al., 2017). The slope of OA to HCHO was higher for wildfires than agricultural fires during SEAC$^4$RS though data were limited (see Table 1). This is consistent with more OA emitted in wildfires than agricultural fires (Liu et al., 2017). The factors driving higher OA to HCHO with wildfires are not clear and may be related to burning conditions and fuels. For the non-BB sources, the slope of OA vs. HCHO was highest for South Korea (KORUS-AQ), which is dominated by heavily polluted anthropogenic sources. During KORUS-AQ, the high OA to HCHO air masses also had high acetonitrile. By the time we sampled, most organic aerosols were secondary (Nault et al., 2018). This indicates that the formation rates of OA and HCHO from different emission sources contribute to the different slopes of OA-HCHO. This also indicates that emission sources with enhanced acetonitrile tend to form more OA relative to HCHO downwind. The slope of OA-HCHO for California LA basin, dominated by relatively clean anthropogenic emissions, was much lower than South Korea. The potential difference in the anthropogenic emissions mix could contribute to the different OA-HCHO slopes from US LA region and South Korea anthropogenic sources (Baker et al., 2008; Na et al., 2005; Na et al., 2002). The slopes of OA vs. HCHO of SEAC$^4$RS and DC3 dominated by biogenic emissions in the SE US were in-between heavily polluted

(KORUS-AQ) and clean anthropogenic sources (CalNex). As SEAC$^4$RS had the largest geographic coverage for low altitude data over US, the campaign average slope of OA vs. HCHO was used to represent the US region in summer. CalNex LA Basin data were used to represent large cities as case studies.

Overall, the source dependent OA-HCHO relationships (Fig. 2) showed higher OA-HCHO slopes of BB and heavily polluted anthropogenic sources with inefficient combustion (e.g., KORUS-AQ) compared to biogenic and relatively clean anthropogenic sources. This indicated that inefficient combustions contribute to the high slopes of OA-HCHO, probably due to both enhanced primary OA and increased formation of SOA. Enhanced pre-existing aerosols such as primary aerosols can provide more surfaces to increase VOCs condensation and SOA formation. VOCs co-emitted from heavily polluted anthropogenic sources can also form more SOA. It is possible to extract the factors that govern the different OA-HCHO relationships and potentially have a universal application of the slopes as a function of the factors (e.g., sources and combustion efficiencies).

### 3.2 Dependence on $NO_x$ and VOCs speciation

Biogenic and anthropogenic VOCs are oxidized by atmospheric oxidants (e.g., OH as the dominant oxidant) to form $RO_2$. HCHO is produced from the reactions of $RO_2$ with $HO_2$ or NO, with $RO_2$+NO typically producing more HCHO than $RO_2 + HO_2$ (e.g., Wolfe et al., 2016). $RO_2$ can react with $HO_2$ or NO, or isomerize to form oxidized organic

compounds with high molecular weight and low volatility, which condense on existing particles to form SOA. The products of $RO_2$ + NO tend to fragment instead of functionalize and often lead to higher volatility compounds (e.g., HCHO) and thus less SOA formation compared to the products of $RO_2$ + $HO_2$ (Kroll et al., 2006; Worton et al., 2013). Therefore, with the same VOC, we expect more HCHO and less OA formed at high NO conditions and vice versa. As mentioned before, $NO_2$ instead of NO is easily measured from space and $NO_2$ typically is ~80% of $NO_x$ in the boundary layer during the day. Therefore, $NO_2$ is used as a surrogate for the NO levels influencing OA and HCHO production. The yields of HCHO and SOA also depend on VOC speciation (e.g., Lee et al., 2006; Bianchi et al., 2016). Specifically, isoprene has a higher yield of HCHO than most non-alkene VOCs (Dufour et al., 2009).

A scatter plot of OA vs. HCHO for SEAC$^4$RS low altitude data is shown in Fig. 3(a). The data are color-coded by the product of in-situ isoprene and $NO_2$, attempting to capture time periods strongly influenced by oxidation products of isoprene at high NO conditions. No trends are evident when the data are instead color coded by $NO_2$ or isoprene only. This may be because isoprene (biogenic source) and $NO_2$ (anthropogenic sources) are generally not co-located in the US (Yu et al., 2016) and isoprene is the dominant source of HCHO compared to anthropogenic VOCs in the US (e.g., Millet et al., 2008). This plot shows that, at high $NO_2$ and high isoprene conditions, less OA was formed for each HCHO produced generally. The correlation coefficient of 0.45 for high $NO_2$ and isoprene conditions during SEAC$^4$RS is not very high but still shows significant dependence of the OA-HCHO relationship on the product of $NO_2$ and isoprene,

considering that these are ambient data and other factors (e.g., different specific sources) also play a role in determining OA-HCHO relationships. This is consistent with high NO and isoprene conditions promote HCHO formation over SOA formation. We also looked at the dependence on peroxy acetyl nitrate (PAN), as PAN is a product of the photo oxidation of VOCs, including isoprene, in the presence of $NO_2$. The dependence on PAN was not as clear as on the product of $NO_2$ and isoprene.

KORUS-AQ OA vs. HCHO, color-coded with $NO_2$, is plotted in Fig. 3(b). The OA-HCHO ratio clearly decreased as $NO_2$ levels increased during KORUS-AQ, suggesting that high NO conditions accelerated HCHO formation more than they did SOA production. OA-HCHO relationships do not have dependence on local time of the day (not shown). This further confirms that $NO_x$ is an important factor that affects the OA-HCHO relationship. Compared to SEAC$^4$RS, the KORUS-AQ OA-HCHO ratio does not depend on VOCs. This may be consistent with the dominant VOCs being anthropogenic VOCs that are co-located with NO sources. This may also suggest that the anthropogenic VOCs generally have a lower HCHO yield than does isoprene. Because OA and HCHO were tightly correlated during CalNex and DC3, we did not parse for $NO_x$. The $NO_x$ range during DC3 low altitude data was smaller than KORUS-AQ and SEAC$^4$RS. DC3 OA-HCHO relationships only had a slight dependence on $NO_2$ (not shown here), largely due to the limited dataset. The $NO_x$ range during CalNex low altitude data was large. The OA and HCHO correlation during CalNex was very tight and the slope of OA-HCHO did not show clear dependence on $NO_x$, which could be due to the combination of different VOCs sources and $NO_x$ levels.

## 4. Comparison of OA-HCHO relationships: in-situ vs. GEOS-Chem

In situ OA-HCHO relationships from SEAC$^4$RS low altitude non-BB (Fig. 4a), KORUS-AQ low altitude (Fig. 4b), and SEAC$^4$RS BB (Fig. 4c) air masses were compared to GEOS-Chem model simulations (Fig. 4d-4f) sampling along the corresponding flight tracks. Similar to the in situ data, GEOS-Chem model simulations also found correlations between OA and HCHO for these three regions, especially for SEAC$^4$RS non-BB. GEOS-Chem was intensively validated with in situ measurements for SE US (e.g., Marais et al., 2016; Kim et al., 2015). The ratios of the slopes between OA and HCHO for the US (SEAC$^4$RS), South Korea (KORUS-AQ), and wildfire cases (SEAC$^4$RS) from GEOS-Chem were 1:1.1:0.4, which was different from the in situ measurements of 1:1.4:13 (Table 1). GEOS-Chem could not capture any wild fires in US during SEAC$^4$RS, which is probably due to poor representation of BB emission inventory for US wildfire and also the coarse grid in GEOS-Chem. GEOS-Chem also significantly under predicted the slope of OA to HCHO for South Korea. We attribute this to a likely underprediction of anthropogenic SOA, which was dominant in South Korea, in GEOS-Chem (Schroder et al., 2018), as well as a different mix of OA and HCHO sources in the US compared to South Korea and representation of these in GEOS-Chem. Although GEOS-Chem contains isoprene chemistry with a focus on the SE US (Marais et al. 2016), there is still room to improve GEOS-Chem model especially for anthropogenic and BB sources, as well as anthropogenic OA formation mechanisms. For example, in the model biogenic sources are more important than anthropogenic sources for the OA and HCHO budgets in South Korea, which is not the case from KORUS-AQ in situ measurements. In

477 the model, a 10% decrease of emissions from biogenic, anthropogenic and BB sources
478 results in a 6%, 3%, and 1% decrease in OA and 2%, 1%, and 0% decrease in HCHO
479 over South Korea in May 2016. However, the in situ airborne field campaign KORUS-
480 AQ found that OA and HCHO were higher near anthropogenic emission sources
481 compared to rural regions. The larger impact of biogenic sources compared to
482 anthropogenic sources on OA and HCHO in the model can be due to both low-biased
483 anthropogenic emission inventories and low-biased anthropogenic SOA. Improving
484 anthropogenic emissions inventories in the models can bring model results closer to
485 observations. Improving anthropogenic SOA, such as implementation of the SIMPLE
486 model, in GEOS-Chem (Hodzic and Jimenez, 2011) can also improve the model results
487 compared to observations. Measurements or measurement-constrained estimation with
488 sufficient spatial and temporal coverage can help to narrow down the key factors (e.g.,
489 emission inventories or chemical schemes) in GEOS-Chem to better represent VOCs and
490 OA globally. Furthermore, we did also find that GEOS-Chem could not capture the
491 observed higher slope of OA to HCHO at high altitudes (not shown), which could be due
492 to issues such as transport, OA lifetime, and OA production.
493
494 **5. Relating satellite HCHO column to surface HCHO concentrations**
495 To utilize the derived in-situ OA-HCHO relationship, the satellite HCHO columns need
496 to be converted to surface HCHO concentrations. We used a vertical distribution factor $\eta$
497 ($cm^{-1}$) (Sect. 2.5), which is defined as the ratio of surface HCHO concentrations (molec
498 $cm^{-3}$) to HCHO column (molec $cm^{-2}$), to estimate surface HCHO concentrations from
499 satellite column measurements. Zhu et al. (2017) used the same vertical distribution

500 factor for their study. The use of this factor is justified by the fact that the derived surface
501 HCHO retained the spatial pattern of the satellite HCHO column and agreed with local
502 surface measurements of HCHO for a multi-year average (Zhu et al., 2017).
503
504 We also investigated the main factors affecting the variation of the vertical distribution
505 factor $\eta$. Because the factor is determined by HCHO vertical distributions, we examined
506 three typical normalized HCHO vertical distribution profiles with the highest, median and
507 lowest $\eta$ values for the SEAC$^4$RS field campaign (Fig. 5). Because the sensitivity of OA
508 estimates to $\eta$ was investigated with $\eta$ from different GEOS-Chem versions (Sect. 6.2),
509 we did not compare HCHO vertical profiles from the model to the measurements from a
510 comprehensive set of field campaigns. We chose SEAC$^4$RS to illustrate the main factors
511 impacting the $\eta$ over US because SEAC$^4$RS had a larger spatial coverage than DC3 and
512 CalNex. GEOS-Chem can generally capture the vertical profiles of measured HCHO.
513 Boundary layer mixing height and surface emission strength are the dominant factors in
514 determining the fraction of HCHO near the surface. Higher boundary layer mixing height
515 results in lower $\eta$ for SE US profiles, where there are biogenic sources of HCHO from
516 the surface and HCHO has distinct concentration difference below and above the
517 boundary layer. However, there are exceptions, such as for the profiles over the ocean
518 and the coastal regions. Although the boundary layer is shallow in these regions, a large
519 portion of HCHO resides above the boundary layer, resulting in low $\eta$. In these cases,
520 surface emissions of HCHO or precursors are very small and therefore methane oxidation
521 makes a large contribution to the total HCHO column. High concentrations of HCHO
522 (e.g., in BB plumes) lofted by convection can also impact the vertical profile (Barth et al.,

523 2015), which is not further investigated because OA estimates with BB influences over
524 US are excluded in current study. Overall, the source intensities and boundary layer
525 mixing height mostly determined the HCHO vertical profiles.
526
527 **6. Construction of the OA estimate**
528 **6.1 Variables to construct OA estimate**
529 As mentioned in Sect. 2.5, the OA estimate value in each grid cell was estimated from
530 monthly average satellite HCHO column observation by the linear Eq. (1). Satellite
531 monthly average HCHO column data, $\Omega_{HCHO}$, were converted to surface HCHO
532 concentrations by multiplying by the $\eta$(i) factor either from climatology a priori profiles
533 or monthly average HCHO profiles. Surface OA was then estimated by multiplying the
534 derived surface HCHO concentrations with the slope $\alpha(i)$ and adding the intercept $\beta$(i).
535 The slope $\alpha(i)$ and intercept $\beta$(i) were determined from the linear regression of in situ
536 OA and HCHO from aircraft field campaign data. The relationship between OA and
537 HCHO varies but previous sections demonstrated that we can quantify the surface OA-
538 HCHO relationship by their regions, sources and chemical conditions (e.g., $NO_x$ and
539 isoprene levels). To test the impact of the chosen OA-HCHO relationship on the
540 calculated OA estimate, the OA estimate in the US was calculated using four different
541 methods (see Table 2). The OA estimate was calculated on the monthly time scale,
542 largely because OA estimate is based on OMI HCHO observations and uncertainty
543 weighted average for a time scale of about one month (Gonzalo et al., 2015; Zhu et al.,
544 2016) is needed to reduce the noise in daily OMI HCHO data. With improved satellite

HCHO data from TROPOMI, higher time resolution (e.g., weekly average) HCHO data could be useful to estimate OA in the future.

**6.2 OA estimate over US**

The monthly average surface OA estimates over the US in August 2013 using SEAC$^4$RS lump-sum slope and intercept (see Table 2) with different $\eta$ are shown in Fig. 6a and 6b. Because BB regions in the US are not covered by smoke continuously during a period of time and it is challenging for satellite retrieval to separate thick BB plumes and clouds without information on the time and location of the burning, thick BB events (OMI UV Aerosol Index (UVAI) > 1.6) (Torres et al., 2007) were excluded and shown as the blank (white) grid cells in Fig. 6a and 6b. The same filter was also applied to aerosol extinction and GEOS-Chem OA abundance. To evaluate the representative quality of the OA estimate, OA estimate data were compared to the EPA IMPROVE ground sites corrected-OA measurements over the US and SEARCH ground sites OA measurements in the SE US (Sect. 2.2). The locations of IMPROVE and SEARCH sites are displayed in Fig. 6e as small and large dots, respectively. The dot color represents the average OA mass concentrations for August 2013.

Considering the uncertainties in satellite HCHO measurements, in using the campaign lump-sum OA-HCHO relationship to represent spatial resolved OA, in HCHO vertical profiles, and in ground IMPROVE network measurements, the correlation (correlation coefficient r = 0.56) between the OA estimate and corrected IMPROVE network measurements (Fig. 6f and 6g) is reasonably good and indicates that the OA estimate can

568 generally capture the variation of OA loading over the US. First, the correlation
569 coefficient between HCHO SAO retrievals and in situ measurements during SEAC$^4$RS
570 was not high (r = 0.24) but this may be partly because they were not sampled at the same
571 time. The uncertainty in HCHO SAO data was likely less than 76%. Second, the
572 uncertainty in applying a campaign lump-sum OA-HCHO relationship to individual
573 spatial resolved satellite HCHO data to estimate OA induced an uncertainty of 41%
574 according to the correlation coefficient of OA-HCHO in the field campaign. Third, $\eta$ in
575 the Fig. 6a OA estimate was from GEOS-Chem v9-02 output for the specific month
576 August, 2013. $\eta$ in the Fig. 6b OA estimate was from GEOS-Chem v9-01-03
577 climatology, the same as satellite data a priori profiles. The good correlations of OA
578 estimates with IMPROVE OA indicate that OA estimates are not very sensitive to $\eta$ from
579 different model versions. The largest difference between the two OA estimates is their
580 concentrations over East Texas. There are no IMPROVE OA measurements in the East
581 Texas to evaluate which works better. Fourth, the uncertainties in IMPROVE OA
582 measurements, such as using a constant correction factor to correct the partial
583 evaporation across all SE US sites, and the spatially dependent OA/OC ratio (Tsigaridis
584 et al., 2014), may also have contributed to the discrepancies between the OA estimate and
585 EPA IMPROVE sites OA. Therefore, higher quality of satellite HCHO data and refining
586 OA-HCHO relationships will help improve our OA estimate products. These combined
587 with a spatially resolved IMPROVE OA correction factor and OA/OC ratios will help
588 improve the correlation coefficients between OA estimates and IMPROVE OA.
589

590 The linear correlation between the OA estimate and IMPROVE OA measurements
591 yielded a slope of 0.62 or 0.60, indicating that the OA estimate underestimated OA. First,
592 the different data collection time for satellite data, in situ measurements and ground
593 observations could contribute to the bias. Satellite HCHO data were measured in mid-
594 day, in situ airborne OA and HCHO were measured during the daytime and IMPROVE
595 network organic carbon was collected day and night. Because ground OA in the SE US
596 were observed to have little diurnal variation (Xu et al., 2015; Hu et al., 2015), the
597 different sampling time of ground and airborne OA probably does not have a significant
598 impact on the comparison of OA estimate and IMPROVE OA. Surface HCHO has
599 evident diurnal profiles with the highest concentrations around the mid-day (Kaiser et al.,
600 2016), which could add uncertainties to OA estimate when using inconsistent time ranges
601 of satellite HCHO data measured in the mid-day and in situ airborne OA-HCHO
602 relationships measured in the daytime. The SEAC$^4$RS HCHO concentrations were
603 converted to 1:30 pm concentrations according to the average HCHO diurnal profile from
604 the Southern Oxidant and Aerosol Study (SOAS) (Kaiser et al., 2016). The OA-HCHO
605 relationship with HCHO converted to 1:30 pm yielded a slope of 5% lower than the
606 original OA-HCHO relationship. Second, the potential uncertainty ($\pm$30%) in OA/OC
607 ratio could also contribute to the systematic difference because we used OA/OC of 2.1
608 and studies (e.g., Pye et al., 2017; Canagaratna et al., 2015) showed that the OA/OC can
609 range from 1.4 to 2.8. Third, the potential underestimation of HCHO from satellite
610 retrieval (by −37%) (Zhu et al., 2016) compared to SEAC$^4$RS may be one of the most
611 important reasons that cause the systematic difference (low slope) between the OA
612 estimate and IMPROVE OA according to Eq. (1). Satellite HCHO data corrected by the

613 low bias (by −37%) (Zhu et al., 2016) will increase our slopes of 0.60-0.62 to be close to
614 the unity.
615
616 SEARCH OA data were also used to compare to the OA estimate. The correlation was
617 good for August 2013. Although the SEARCH network OA measurements have better
618 accuracy, the number of SEARCH sites is limited (5 sites). The correlation of OA
619 estimate and SEARCH OA varied dramatically 2008-2013 (Fig. S1). GEOS-Chem OA
620 did not correlate with SEARCH OA except for the year 2013 (Fig. S1). As the
621 IMPROVE network has more sites and spatial coverage, we used IMPROVE network
622 data as ground OA measurements for comparison in the remainder of the discussion.
623
624 **6.3 Comparison to aerosol extinction from AOD**
625 To further evaluate the method of using satellite HCHO to derive an OA surface estimate,
626 satellite aerosol measurements were used to approximate surface OA extinction for
627 comparison. Satellite measurements of AOD were converted to surface extinction (see
628 Sec. 2.6). Studies showed that OA were a dominant component of aerosol mass and
629 extinction during SEAC$^4$RS (Kim et al., 2015; Wagner et al., 2015) and the fractions of
630 OA were relatively constant (interdecile 62-74%) (Wagner et al., 2015). Therefore AOD
631 variation is expected to generally reflect the OA variation during SEAC$^4$RS. Satellite
632 measurements from MISR can provide more aerosol property information to apportion
633 total AOD to AOD of a subset of aerosols with small to medium size and round shape,
634 which can better capture OA, when AOD is above 0.15 to 0.2 (Kahn and Gaitley, 2015;
635 personal communication with R. Kahn, 2018). Because MISR cannot distinguish OA and

636 other submicron aerosol components (e.g., sulfate and nitrate) and would cut off low
637 AOD data which accounted for near half of the data over US, we used total AOD to
638 derive extinction for our comparison. The AOD-derived extinction map is shown in Fig.
639 6(c), and the scatter plot of AOD-derived extinction and EPA corrected OA is displayed
640 in Fig. 6(h). The same filter of high AI was also applied to AOD-derived extinction to
641 remove BB plumes. Generally, the derived aerosol extinction had a correlation with
642 IMPROVE OA, but the correlation was not as good as for the OA estimate with
643 IMPROVE OA. The high surface aerosol extinctions (> 150 $Mm^{-1}$) (outliners in the
644 scatter plot) were located in the SE US and therefore were not due to potential
645 contribution of dust and nitrate altering the shape of vertical profiles outside of the SE
646 US. This indicates that the OA estimate derived from HCHO may be better than AOD at
647 representing the concentrations of OA, even for the regions where AOD is dominated by
648 OA (Xu et al., 2015).
649
650 **6.4 Comparison to GEOS-Chem OA**
651 Surface OA over the US from a GEOS-Chem simulation for August 2013 is shown in
652 Fig. 6(d), and the scatter plot of GEOS-Chem OA with IMPROVE OA is in Fig. 6(i).
653 Although HCHO vertical profiles from GEOS-Chem were used in OA estimate, the
654 GEOS-Chem simulation had a coarser resolution than OA estimate. To be comparable to
655 the OA estimate, the scatter plot Fig. 6(i) used GEOS-Chem results for the grid squares
656 that overlaped with individual IMPROVE sites. Compared to the OA estimate, GEOS-
657 Chem OA had a similar correlation coefficient with IMPROVE OA. Although the
658 GEOS-Chem OA plot appeared more scattered, there were many GEOS-Chem data

points close to zero when IMPROVE OA was low, making the overall correlation coefficient similar to that for the OA estimate. GEOS-Chem under predicted IMPROVE OA more with a slope of 0.57 compared to the OA estimate. This is consistent with underprediction of anthropogenic OA in Marais et al. (2016).

**6.5 OA estimate with different OA-HCHO relationships**

OA were estimated with different OA-HCHO relationships for 4 cases (Table 2). LUMP-SUM was using the non-BB SEAC$^4$RS campaign lump-sum relationship, the same as shown in Fig. 6; ISOP-NOx was using non-BB SEAC$^4$RS $NO_2$ and isoprene dependent relationship; URBAN was using CalNex for large urban cities and SEAC$^4$RS lump-sum for other US regions; and COMBINE was using CalNex for large urban cities and $NO_2$ and isoprene dependent non-BB SEAC$^4$RS for other US regions. The OA estimates from the 4 cases (Table 2) were compared to IMPROVE OA and the correlation coefficients are shown in Fig. 7. In general, OA estimate results from the four cases were similar.

The details about how to implement chemical factors dependent OA estimates for the four cases are also provided in Table 2. Including the $NO_2$–isoprene-dependent OA-HCHO relationship (ISOP-NOx case) showed a similar (or slightly worse) correlation between the OA estimate and IMPROVE OA. OMI $NO_2$ column observations were used to represent surface $NO_2$ levels and surface isoprene emissions from MEGAN were used to represent surface isoprene concentrations, assuming that $NO_2$ column observations reflect surface $NO_2$ distributions and isoprene emissions reflect the concentrations of isoprene due to its short lifetime (~1 hr). The detailed implementation is provided in the

682 notes in Table 2. As the in situ data showed a moderate $NO_2$-isoprene-dependent OA-
683 HCHO relationship, we attributed this to the locations of IMPROVE site at rural regions,
684 the uncertainty in IMPROVE network measurements, the uncertainty in isoprene
685 emissions from MEGAN, or factors (e.g., source-dependent OA-HCHO) that also need to
686 be taken into account when determining the specific OA-HCHO relationship. Satellite
687 OMI $NO_2$ data (at 1 : 30 pm) were used to represent $NO_2$ levels, big cities were defined
688 as $NO_2 > 4 \times 10^{15}$ molec $cm^{-2}$, and the CalNex in situ OA-HCHO relationship was
689 applied for big cities. It turned out that only 1 IMPROVE site (San Gabriel, SAGA1) near
690 LA was affected by high $NO_2$ and led to the insignificant change in URBAN compared to
691 LUMP-SUM. This is not unexpected because IMPROVE sites are in rural regions. The
692 OA estimate in SAGA1 decreased from 1.88 μg $m^{-3}$ from LUMP-SUM to 0.17 μg $m^{-3}$ in
693 URBAN while the measured OA in IMPROVE SAGA1 was 1.52 μg $m^{-3}$. This may infer
694 that CalNex is not very consistent with SEAC$^4$RS due to different sampling instruments,
695 strategies and seasons. Lowing the $NO_2$ threshold when defining big cities did not help
696 improve the agreement either.
697
698 Because separating large urban areas and other regions and applying a simple chemical
699 regime dependent in situ OA-HCHO relationship did not improve the agreement between
700 the OA estimate and IMPROVE OA, we used the lump-sum OA-HCHO relationship to
701 derive the OA estimate (shown in Fig. 6). SEAC$^4$RS and DC3 only had a few low altitude
702 data in the Midwest and did not cover the Northeast US. The measured OA-HCHO
703 relationship in the Midwest did not show significant difference from the SE US. The
704 scatter plots (Fig. 6f and 6g) of OA estimates and IMPROVE OA do not show outliners

705 for the Northeast and Midwest. This indicates that using the SEAC$^4$RS lump-sum OA-
706 HCHO relationship can reasonably capture regions outside of the SE US.
707
708 **6.6 Temporal variation of the agreement between OA estimate and IMPROVE OA**
709 Besides August 2013 (see Fig. 6), the correlations between the OA estimate and
710 IMPROVE OA for the summer months June-July-August 2008-2013 were also examined
711 and shown in Fig. 7. Generally, the correlation coefficients between the OA estimate and
712 IMPROVE OA were >0.5 for summer months of the years investigated. The correlation
713 coefficients were generally higher in June compared to July and August. The lower
714 average temperature in June might be related to the higher correlation coefficients.
715 IMPROVE network aerosol samples were transported at ambient temperature in a truck
716 and more organic vapors likely evaporated at higher temperature. The different
717 temperatures and distances from IMPROVE sites to the laboratory may lead to
718 inhomogeneous evaporation among the samples and result in lower correlation
719 coefficients. Although higher temperatures in July and August may also lead to more BB,
720 average aerosol index over the US was not higher in July (mean: 0.35) and August
721 (mean: 0.36) compared to June (mean: 0.39) for these years. The underlying cause for the
722 lowest correlation coefficients in July and August 2012 is not clear and may be related to
723 the severe drought in 2012 (Seco et al., 2015). The correlation coefficients were also low
724 for the linear regressions (not shown) of IMPROVE OA with both GEOS-Chem OA and
725 AOD-derived extinction. Because the lowest correlation coefficients were consistently
726 observed for multiple OA-related products and not just the OA estimate, we attributed

727 this to uncertainties in the IMPROVE OA measurements or some unknown bias shared
728 by the satellite HCHO, GEOS-Chem OA, and satellite AOD.
729
730 **6.7 South Korea OA estimate**
731 We attempted to estimate an OA estimate for South Korea, using airborne in situ
732 measurements of OA and HCHO from the KORUS-AQ field campaign (Aknan and
733 Chen, 2017) and SAO OMI HCHO measurements. The National Institute of
734 Environmental Research (NIER) ground sites OC measurements during KORUS-AQ
735 over South Korea could be used to validate the OA estimate. However, OMI HCHO
736 measurements were below the detection limit (Zhu et al., 2016) in May 2016. Also, there
737 were no OMI data available in June 2016 when airborne measurements and ground sites
738 OC measurements were available during KORUS-AQ. Because an OA estimate for South
739 Korea could not be well retrieved and validated, it was not presented in this study.
740 Although an OA estimate for South Korea could not be retrieved in the current study, the
741 consistency in the dependence of OA-HCHO relationships on chemical factors (e.g.,
742 emission sources, $NO_x$, and altitudes) provides important information for potential
743 application of chemical factors dependent OA-HCHO relationships to the geographical
744 domain beyond the continental US, especially with improved satellite HCHO data from
745 Tropospheric Monitoring Instrument (TROPOMI).
746
747 **7 Limitations of the OA estimate and future work**
748 Because the OA estimate is based on satellite HCHO data, the detection limit of satellite
749 HCHO data affects the quality of the OA estimate. Currently, due to the limited

sensitivity of OMI for HCHO, the OA estimate is valid only when high levels of HCHO are present, such as during summer time and near large HCHO sources. With the new TROPOMI satellite instrument and future missions TEMPO and GEMS, satellite HCHO measurements will have higher spatial and temporal resolutions and lower detection limits. These higher quality satellite HCHO measurements will improve the quality and spatial and temporal coverage of our OA estimate.

Because the OA estimate uses the relationship of in situ HCHO and OA measurements, the coverage of in situ aircraft field campaigns will impact the OA estimate quality. Currently, in situ airborne measurements of OA and HCHO focus on the continental US. Extending measurements to regions such as Africa BB, South America, and East Asia, where HCHO and OA have high concentrations, will increase the spatial coverage of the OA estimate product. Ground site measurements of OA with consistent quality control in those regions will also be important for validating the OA estimate.

Improvement of satellite HCHO retrieval during the BB cases will also improve OA estimate quality. BB cases with high UV aerosol index over the US were excluded in the current OA estimate. With improvement in the satellite retrieval of HCHO, we may be able to estimate OA during BB cases over the US. Upcoming field campaigns such as the Fire Influence on Regional and Global Environments Experiment - Air Quality (FIREX-AQ) will provide opportunities to improve the OA estimate in BB cases in the US.

772 This OA estimate method has limitations in remote regions far away from HCHO
773 sources. Because the lifetimes of HCHO (1-3 hours) and OA (1 week) are different, the
774 slopes and intercepts between HCHO and OA are expected to change when air masses
775 are aged (e.g., in remote regions). HCHO is close to being in steady-state with production
776 rates roughly equal to loss rates while OA is not in steady-state with a lifetime of a week.
777 Therefore, OA can be accumulated relative to HCHO when air masses are aged. OA vs.
778 HCHO from SEAC$^4$RS and KORUS-AQ field campaigns, color-coded with altitude as an
779 indicator of air mass age, are plotted in Fig. S2 (a) and (b), respectively. A relative
780 depletion of HCHO at high altitudes was observed due to its shorter lifetime. This also
781 suggests that, at remote regions far away from the sources, the ratios of OA and HCHO
782 could be much higher and the relationship between OA and HCHO derived near the
783 sources may no longer apply. On the other hand, the lifetime of 1-3 hrs for HCHO does
784 not imply that the OA estimate only work within this timescale. HCHO is formed from
785 oxidation of transported gas phase VOCs, including the oxidation products of the primary
786 emitted VOCs, as well as of the slower reacting VOCs (e.g., Ethane and Benzene). Most
787 gas-to-particle oxidation processes that might produce HCHO can last up to 1-2 days
788 (Palm et al., 2018). Fig. S3 shows the ratios of OA and HCHO did not change
789 significantly downwind for the Rim Fire plume for about 1 day of aging, which was
790 determined by the distance from the source and the wind speed. A lower photolysis rate
791 of HCHO in the plume can also contribute to this. However, we do not expect the
792 relationship of OA and HCHO to remain past 1-2 boundary layer ventilation cycles (Palm
793 et al., 2018). Although OA-HCHO relationships depend on air mass age, it does not
794 largely affect our study for monthly average surface OA over continental US because our

OA estimates showed reasonably good agreement with ground sites IMPROVE OA measurements. This also indicates that SOA are enhanced near the source regions statistically. Nault et al. (2018) also showed the production of HCHO and SOA are similar and plateau around 0.5 – 1 photochemical day. So, in the near field of emissions and chemistry, the productions of these two species are similar; however, outside of near field of emissions and rapid chemistry, the long lifetime of OA vs the steady state of HCHO would start controlling the slopes and correlations.

## 8 Summary

We have developed a satellite-based estimate of the surface OA concentration ("OA estimate") based on in situ observations. This estimate is based on the empirical relationships of in-situ OA and HCHO for several regions. OA and HCHO share VOC sources with different yields and lifetimes. Using surface OA and HCHO linear regression slopes and intercepts we can relate surface HCHO to OA. To estimate the surface HCHO concentration from satellite HCHO column, we used a vertical distribution factor $\eta$ from either climatology satellite data a priori profiles or updated model run for specific period, which is largely determined by boundary layer height and surface emissions and found to reasonably retrieve surface HCHO from column HCHO.

The OA estimate over the continental US generally correlated well with EPA IMPROVE network OA measurements corrected for partial evaporation, with a biased low slope of 0.62 or 0.60, mostly due to underestimation of HCHO concentrations from the OMI

HCHO retrieval. The good correlations are not only for the time during SEAC$^4$RS but also for most summer months over several years (2008-2013) investigated. Compared to aerosol extinction derived from AOD, the OA estimate had slightly higher correlation coefficients with IMPROVE OA. GEOS-Chem can predict OA with a similar correlation coefficient with IMPROVE OA compared to the OA estimate when GEOS-Chem was intensively validated with in situ measurements for SE US. Better satellite HCHO data from TROPOMI and future TEMPO and GEMS and extending spatiotemporal coverage of in situ measurements will improve the quality and coverage of the OA estimate.

**Acknowledgements:**

JL, TFH, GMW, and JSC were supported by NASA grant NNH15ZDA001N and NNH10ZDA001N. BAN, PCJ, and JLJ were supported by NASA grant NNX15AT96G and 80NSSC18K0630. AW and PTR-MS measurements during DC3, SEAC$^4$RS and KORUS-AQ were supported by the Austrian Federal Ministry for Transport, Innovation and Technology (bmvit) through the Austrian Space Applications Programme (ASAP) of the Austrian Research Promotion Agency (FFG). The PTR-MS instrument team (P. Eichler, L. Kaser, T. Mikoviny, M. Müller) is acknowledged for their field support. We thank E. Edgerton for providing the SEARCH network data.

References:


Aknan, A. and Chen, G.: KORUS-AQ DC-8 Aircraft Dataset, available at: https://www-air.larc.nasa.gov/cgi-bin/ArcView/korusaq, last access: 3 February 2017.

Anderson, D. C., Loughner, C. P., Diskin, G., Weinheimer, A., Canty, T. P., Salawitch, R. J., Worden, H. M., Fried, A., Mikoviny, T., Wisthaler, A., and Dickerson, R. R.: Measured and modeled CO and NOy in DISCOVER-AQ: An evaluation of emissions and chemistry over the eastern US, Atmos Environ, 96, 78-87, 10.1016/j.atmosenv.2014.07.004, 2014.

Attwood, A. R., Washenfelder, R. A., Brock, C. A., Hu, W., Baumann, K., Campuzano-Jost, P., Day, D. A., Edgerton, E. S., Murphy, D. M., Palm, B. B., McComiskey, A., Wagner, N. L., de Sa, S. S., Ortega, A., Martin, S. T., Jimenez, J. L., and Brown, S. S.: Trends in sulfate and organic aerosol mass in the Southeast U.S.: Impact on aerosol optical depth and radiative forcing, Geophys Res Lett, 41, 7701-7709, 10.1002/2014gl061669, 2014.

Bahreini, R., Middlebrook, A. M., de Gouw, J. A., Warneke, C., Trainer, M., Brock, C. A., Stark, H., Brown, S. S., Dube, W. P., Gilman, J. B., Hall, K., Holloway, J. S., Kuster, W. C., Perring, A. E., Prevot, A. S. H., Schwarz, J. P., Spackman, J. R., Szidat, S., Wagner, N. L., Weber, R. J., Zotter, P., and Parrish, D. D.: Gasoline emissions dominate over diesel in formation of secondary organic aerosol mass, Geophys Res Lett, 39, Artn L06805 10.1029/2011gl050718, 2012.

Baker, A. K., Beyersdorf, A. J., Doezema, L. A., Katzenstein, A., Meinardi, S., Simpson, I. J., Blake, D. R., and Rowland, F. S.: Measurements of nonmethane hydrocarbons in 28 United States cities, Atmos Environ, 42, 170-182, 10.1016/j.atmosenv.2007.09.007, 2008.

Barth, M. C., Cantrell, C. A., Brune, W. H., Rutledge, S. A., Crawford, J. H., Huntrieser, H., Carey, L. D., MacGorman, D., Weisman, M., Pickering, K. E., Bruning, E., Anderson, B., Apel, E., Biggerstaff, M., Campos, T., Campuzano-Jost, P., Cohen, R., Crounse, J., Day, D. A., Diskin, G., Flocke, F., Fried, A., Garland, C., Heikes, B., Honomichl, S., Hornbrook, R., Huey, L. G., Jimenez, J. L., Lang, T., Lichtenstern, M., Mikoviny, T., Nault, B., O'Sullivan, D., Pan, L. L., Peischl, J., Pollack, I., Richter, D., Riemer, D., Ryerson, T., Schlager, H., St Clair, J., Walega, J., Weibring, P., Weinheimer, A., Wennberg, P., Wisthaler, A., Wooldridge, P. J., and Ziegler, C.: The Deep Convective Clouds and Chemistry (Dc3) Field Campaign, B Am Meteorol Soc, 96, 1281-1309, 10.1175/Bams-D-13-00290.1, 2015.

Bianchi, F., Barmet, P., Stirnweis, L. El Haddad, I., Platt, S.M., Saurer, M., Lötscher, C., Siegwolf, R., Bigi, A., Hoyle, C.R., DeCarlo, P.F., Slowik, J.G., Prévôt, A.S.H., Baltensperger, U., and Dommen. Contribution of methane to aerosol carbon mass. Atmospheric Environment, 141, 41-47, doi: 10.1016/j.atmosenv.2016.06.036, 2016.

Canagaratna, M. R., Jayne, J. T., Jimenez, J. L., Allan, J. D., Alfarra, M. R., Zhang, Q., Onasch, T. B., Drewnick, F., Coe, H., Middlebrook, A., Delia, A., Williams, L. R., Trimborn, A. M., Northway, M. J., DeCarlo, P. F., Kolb, C. E., Davidovits, P., and Worsnop, D. R.: Chemical and microphysical characterization of ambient aerosols with the aerodyne aerosol mass spectrometer, Mass Spectrom Rev, 26, 185-222, 10.1002/mas.20115, 2007.

Canagaratna, M. R., Jimenez, J. L., Kroll, J. H., Chen, Q., Kessler, S. H., Massoli, P., Hildebrandt Ruiz, L., Fortner, E., Williams, L. R., Wilson, K. R., Surratt, J. D., Donahue, N. M., Jayne, J. T., and Worsnop, D. R.: Elemental ratio measurements of organic compounds using aerosol mass spectrometry: characterization, improved calibration, and implications, Atmos Chem Phys, 15, 253-272, https://doi.org/10.5194/acp-15-253-2015, 2015.

Carslaw, K. S., Lee, L. A., Reddington, C. L., Pringle, K. J., Rap, A., Forster, P. M., Mann, G. W., Spracklen, D. V., Woodhouse, M. T., Regayre, L. A., and Pierce, J. R.: Large contribution of natural aerosols to uncertainty in indirect forcing, Nature, 503, 67-+, 10.1038/nature12674, 2013.

Cazorla, M., Wolfe, G. M., Bailey, S. A., Swanson, A. K., Arkinson, H. L., and Hanisco, T. F.: A new airborne laser-induced fluorescence instrument for in situ detection of formaldehyde throughout the troposphere and lower stratosphere, Atmos Meas Tech, 8, 541-552, 10.5194/amt-8-541-2015, 2015.

Cubison, M. J., Ortega, A. M., Hayes, P. L., Farmer, D. K., Day, D., Lechner, M. J., Brune, W. H., Apel, E., Diskin, G. S., Fisher, J. A., Fuelberg, H. E., Hecobian, A., Knapp, D. J., Mikoviny, T., Riemer, D., Sachse, G. W., Sessions, W., Weber, R. J., Weinheimer, A. J., Wisthaler, A., and Jimenez, J. L.: Effects of aging on organic aerosol from open biomass burning smoke in aircraft and laboratory studies, Atmos. Chem. Phys., 11, 12049-12064, https://doi.org/10.5194/acp-11-12049-2011, 2011.

Day, D. A., Wooldridge, P. J., Dillon, M. B., Thornton, J. A., and Cohen, R. C.: A thermal dissociation laser-induced fluorescence instrument for in situ detection of NO2, peroxy nitrates, alkyl nitrates, and HNO3, J Geophys Res-Atmos, 107, Artn 4046 10.1029/2001jd000779, 2002.

de Vries, M. J. M. P., Beirle, S., Hormann, C., Kaiser, J. W., Stammes, P., Tilstra, L. G., Tuinder, O. N. E., and Wagner, T.: A global aerosol classification algorithm incorporating multiple satellite data sets of aerosol and trace gas abundances, Atmos Chem Phys, 15, 10597-10618, 10.5194/acp-15-10597-2015, 2015.

DeCarlo, P. F., Kimmel, J. R., Trimborn, A., Northway, M. J., Jayne, J. T., Aiken, A. C., Gonin, M., Fuhrer, K., Horvath, T., Docherty, K. S., Worsnop, D. R., and Jimenez, J. L.: Field-deployable, high-resolution, time-of-flight aerosol mass spectrometer, Anal Chem, 78, 8281-8289, 10.1021/ac061249n, 2006.

DeCarlo, P. F., Ulbrich, I. M., Crounse, J., de Foy, B., Dunlea, E. J., Aiken, A. C., Knapp, D., Weinheimer, A. J., Campos, T., Wennberg, P. O., and Jimenez, J. L.: Investigation of the sources and processing of organic aerosol over the Central Mexican Plateau from aircraft measurements during MILAGRO, Atmos. Chem. Phys., 10, 5257-5280, https://doi.org/10.5194/acp-10-5257-2010, 2010.

Dufour, G.,, Wittrock, F., Camredon, M., Beekmann, M., Richter, A., Aumont, B., Burrows, J.P., SCIAMACHY formaldehyde observations: constraint for isoprene emission estimates over

Europe? Atmos Chem Phys, 9,1647–1664, 2009.

Drewnick, F., Hings, S. S., DeCarlo, P., Jayne, J. T., Gonin, M., Fuhrer, K., Weimer, S., Jimenez, J. L., Demerjian, K. L., Borrmann, S., and Worsnop, D. R.: A new time-of-flight aerosol mass spectrometer (TOF-AMS) - Instrument description and first field deployment, Aerosol Sci Tech, 39, 637-658, 10.1080/02786820500182040, 2005.

Dunlea, E. J., DeCarlo, P. F., Aiken, A. C., Kimmel, J. R., Peltier, R. E., Weber, R. J., Tomlinson, J., Collins, D. R., Shinozuka, Y., McNaughton, C. S., Howell, S. G., Clarke, A. D., Emmons, L. K., Apel, E. C., Pfister, G. G., van Donkelaar, A., Martin, R. V., Millet, D. B., Heald, C. L., and Jimenez, J. L.: Evolution of Asian aerosols during transpacific transport in INTEX-B, Atmos Chem Phys, 9, 7257-7287, DOI 10.5194/acp-9-7257-2009, 2009.

Edgerton, E. S., Hartsell, B. E., Saylor, R. D., Jansen, J. J., Hansen, D. A., and Hidy, G. M.: The Southeastern Aerosol Research and Characterization Study, part 3: Continuous measurements of fine particulate matter mass and composition, J Air Waste Manage, 56, 1325-1341, Doi 10.1080/10473289.2006.10464585, 2006.

Gelaro, R., McCarty, W., Suarez, M. J., Todling, R., Molod, A., Takacs, L., Randles, C. A., Darmenov, A., Bosilovich, M. G., Reichle, R., Wargan, K., Coy, L., Cullather, R., Draper, C., Akella, S., Buchard, V., Conaty, A., da Silva, A. M., Gu, W., Kim, G. K., Koster, R., Lucchesi, R., Merkova, D., Nielsen, J. E., Partyka, G., Pawson, S., Putman, W., Rienecker, M., Schubert, S. D., Sienkiewicz, M., and Zhao, B.: The Modern-Era Retrospective Analysis for Research and Applications, Version 2 (MERRA-2), J Climate, 30, 5419-5454, 10.1175/Jcli-D-16-0758.1, 2017.

Giglio, L., Randerson, J. T., and van der Werf, G. R.: Analysis of daily, monthly, and annual burned area using the fourth-generation global fire emissions database (GFED4): J. Geophys. Res.-Biogeo., 118, 317–328, https://doi.org/10.1002/jgrg.20042, 2013.

Gonzalez Abad, G. G., Liu, X., Chance, K., Wang, H., Kurosu, T. P., and Suleiman, R.: Updated Smithsonian Astrophysical Observatory Ozone Monitoring Instrument (SAO OMI) formaldehyde retrieval, Atmos Meas Tech, 8, 19-32, 10.5194/amt-8-19-2015, 2015.

Guenther, A., Karl, T., Harley, P., Wiedinmyer, C., Palmer, P. I., and Geron, C.: Estimates of global terrestrial isoprene emissions using MEGAN (Model of Emissions of Gases and Aerosols from Nature), Atmos Chem Phys, 6, 3181-3210, DOI 10.5194/acp-6-3181-2006, 2006.

Hand, J. L., Schichtel, B. A., Malm, W. C., and Frank, N. H.: Spatial and Temporal Trends in PM2.5 Organic and Elemental Carbon across the United States, Adv Meteorol, Artn 367674, 10.1155/2013/367674, 2013.

Hand, J. L., Schichtel, B. A., Malm, W. C., Pitchford, M., and Frank, N. H.: Spatial and seasonal patterns in urban influence on regional concentrations of speciated aerosols across the United States, J Geophys Res-Atmos, 119, 12832-12849, 10.1002/2014jd022328, 2014.

Harvard-Smithsonia Center for Astrophysics, OMI HCHO data product description:

https://www.cfa.harvard.edu/atmosphere/Instruments/OMI/PGEReleases/READMEs/OMHCHO_README_v3.0.pdf, last accessed: 22 January, 2019.

Hayes, P. L., Carlton, A. G., Baker, K. R., Ahmadov, R., Washenfelder, R. A., Alvarez, S., Rappenglück, B., Gilman, J. B., Kuster, W. C., de Gouw, J. A., Zotter, P., Prévôt, A. S. H., Szidat, S., Kleindienst, T. E., Offenberg, J. H., Ma, P. K., and Jimenez, J. L.: Modeling the formation and aging of secondary organic aerosols in Los Angeles during CalNex 2010, Atmos. Chem. Phys., 15, 5773-5801, https://doi.org/10.5194/acp-15-5773-2015, 2015.

Hayes, P. L., Ortega, A. M., Cubison, M. J., Froyd, K. D., Zhao, Y., Cliff, S. S., Hu, W. W., Toohey, D. W., Flynn, J. H., Lefer, B. L., Grossberg, N., Alvarez, S., Rappenglueck, B., Taylor, J. W., Allan, J. D., Holloway, J. S., Gilman, J. B., Kuster, W. C., De Gouw, J. A., Massoli, P., Zhang, X., Liu, J., Weber, R. J., Corrigan, A. L., Russell, L. M., Isaacman, G., Worton, D. R., Kreisberg, N. M., Goldstein, A. H., Thalman, R., Waxman, E. M., Volkamer, R., Lin, Y. H., Surratt, J. D., Kleindienst, T. E., Offenberg, J. H., Dusanter, S., Griffith, S., Stevens, P. S., Brioude, J., Angevine, W. M., and Jimenez, J. L.: Organic aerosol composition and sources in Pasadena, California, during the 2010 CalNex campaign, J Geophys Res-Atmos, 118, 9233-9257, 10.1002/jgrd.50530, 2013.

Heald, C. L., Coe, H., Jimenez, J. L., Weber, R. J., Bahreini, R., Middlebrook, A. M., Russell, L. M., Jolleys, M., Fu, T. M., Allan, J. D., Bower, K. N., Capes, G., Crosier, J., Morgan, W. T., Robinson, N. H., Williams, P. I., Cubison, M. J., DeCarlo, P. F., and Dunlea, E. J.: Exploring the vertical profile of atmospheric organic aerosol: comparing 17 aircraft field campaigns with a global model, Atmos Chem Phys, 11, 12673-12696, 10.5194/acp-11-12673-2011, 2011.

Heald, C. L., Goldstein, A. H., Allan, J. D., Aiken, A. C., Apel, E., Atlas, E. L., Baker, A. K., Bates, T. S., Beyersdorf, A. J., Blake, D. R., Campos, T., Coe, H., Crounse, J. D., DeCarlo, P. F., de Gouw, J. A., Dunlea, E. J., Flocke, F. M., Fried, A., Goldan, P., Griffin, R. J., Herndon, S. C., Holloway, J. S., Holzinger, R., Jimenez, J. L., Junkermann, W., Kuster, W. C., Lewis, A. C., Meinardi, S., Millet, D. B., Onasch, T., Polidori, A., Quinn, P. K., Riemer, D. D., Roberts, J. M., Salcedo, D., Sive, B., Swanson, A. L., Talbot, R., Warneke, C., Weber, R. J., Weibring, P., Wennberg, P. O., Worsnop, D. R., Wittig, A. E., Zhang, R., Zheng, J., and Zheng, W.: Total observed organic carbon (TOOC) in the atmosphere: a synthesis of North American observations, Atmos Chem Phys, 8, 2007-2025, 10.5194/acp-8-2007-2008, 2008.

Hidy, G. M., Blanchard, C. L., Baumann, K., Edgerton, E., Tanenbaum, S., Shaw, S., Knipping, E., Tombach, I., Jansen, J., and Walters, J.: Chemical climatology of the southeastern United States, 1999-2013, Atmos Chem Phys, 14, 11893-11914, 10.5194/acp-14-11893-2014, 2014.

Hodzic, A., and Jimenez, J. L.: Modeling anthropogenically controlled secondary organic aerosols in a megacity: a simplified framework for global and climate models, Geosci Model Dev, 4, 901-917, 10.5194/gmd-4-901-2011, 2011.

Hu, W. W., Campuzano-Jost, P., Palm, B. B., Day, D. A., Ortega, A. M., Hayes, P. L., Krechmer, J. E., Chen, Q., Kuwata, M., Liu, Y. J., de Sá, S. S., McKinney, K., Martin, S. T., Hu, M., Budisulistiorini, S. H., Riva, M., Surratt, J. D., St. Clair, J. M., Isaacman-Van Wertz, G.,

Yee, L. D., Goldstein, A. H., Carbone, S., Brito, J., Artaxo, P., de Gouw, J. A., Koss, A., Wisthaler, A., Mikoviny, T., Karl, T., Kaser, L., Jud, W., Hansel, A., Docherty, K. S., Alexander, M. L., Robinson, N. H., Coe, H., Allan, J. D., Canagaratna, M. R., Paulot, F., and Jimenez, J. L.: Characterization of a real-time tracer for isoprene epoxydiols-derived secondary organic aerosol (IEPOX-SOA) from aerosol mass spectrometer measurements, Atmos. Chem. Phys., 15, 11807-11833, https://doi.org/10.5194/acp-15-11807-2015, 2015.

Hudson, P. K., Murphy, D. M., Cziczo, D. J., Thomson, D. S., de Gouw, J. A., Warneke, C., Holloway, J., Jost, J. R., and Hubler, G.: Biomass-burning particle measurements: Characteristic composition and chemical processing, J Geophys Res-Atmos, 109, Artn D23s27 10.1029/2003jd004398, 2004.

Jimenez, J. L., Canagaratna, M. R., Donahue, N. M., Prevot, A. S. H., Zhang, Q., Kroll, J. H., DeCarlo, P. F., Allan, J. D., Coe, H., Ng, N. L., Aiken, A. C., Docherty, K. S., Ulbrich, I. M., Grieshop, A. P., Robinson, A. L., Duplissy, J., Smith, J. D., Wilson, K. R., Lanz, V. A., Hueglin, C., Sun, Y. L., Tian, J., Laaksonen, A., Raatikainen, T., Rautiainen, J., Vaattovaara, P., Ehn, M., Kulmala, M., Tomlinson, J. M., Collins, D. R., Cubison, M. J., Dunlea, E. J., Huffman, J. A., Onasch, T. B., Alfarra, M. R., Williams, P. I., Bower, K., Kondo, Y., Schneider, J., Drewnick, F., Borrmann, S., Weimer, S., Demerjian, K., Salcedo, D., Cottrell, L., Griffin, R., Takami, A., Miyoshi, T., Hatakeyama, S., Shimono, A., Sun, J. Y., Zhang, Y. M., Dzepina, K., Kimmel, J. R., Sueper, D., Jayne, J. T., Herndon, S. C., Trimborn, A. M., Williams, L. R., Wood, E. C., Middlebrook, A. M., Kolb, C. E., Baltensperger, U., and Worsnop, D. R.: Evolution of Organic Aerosols in the Atmosphere, Science, 326, 1525-1529, 10.1126/science.1180353, 2009.

Jimenez, J. L., Canagaratna, M. R., Drewnick, F., Allan, J. D., Alfarra, M. R., Middlebrook, A. M., Slowik, J. G., Zhang, Q., Coe, H., Jayne, J. T., and Worsnop, D. R.: Comment on "The effects of molecular weight and thermal decomposition on the sensitivity of a thermal desorption aerosol mass spectrometer", Aerosol Sci Tech, 50, I-Xv, 10.1080/02786826.2016.1205728, 2016.

Kahn, R. A., and Gaitley, B. J.: An analysis of global aerosol type as retrieved by MISR, J Geophys Res-Atmos, 120, 4248-4281, 10.1002/2015jd023322, 2015.

Kaiser, J., Jacob, D. J., Zhu, L., Travis, K. R., Fisher, J. A., Abad, G. G., Zhang, L., Zhang, X. S., Fried, A., Crounse, J. D., St Clair, J. M., and Wisthaler, A.: High-resolution inversion of OMI formaldehyde columns to quantify isoprene emission on ecosystem-relevant scales: application to the southeast US, Atmos Chem Phys, 18, 5483-5497, 10.5194/acp-18-5483-2018, 2018.

Kaiser, J., Skog, K. M., Baumann, K., Bertman, S. B., Brown, S. B., Brune, W. H., Crounse, J. D., de Gouw, J. A., Edgerton, E. S., Feiner, P. A., Goldstein, A. H., Koss, A., Misztal, P. K., Nguyen, T. B., Olson, K. F., St Clair, J. M., Teng, A. P., Toma, S., Wennberg, P. O., Wild, R. J., Zhang, L., and Keutsch, F. N.: Speciation of OH reactivity above the canopy of an isoprene-dominated forest, Atmos Chem Phys, 16, 9349-9359, 2016.

Kiehl, J. T., and Briegleb, B. P.: The Relative Roles of Sulfate Aerosols and Greenhouse Gases in Climate Forcing, Science, 260, 311-314, DOI 10.1126/science.260.5106.311, 1993.

Kim, P. S., Jacob, D. J., Fisher, J. A., Travis, K., Yu, K., Zhu, L., Yantosca, R. M., Sulprizio, M. P., Jimenez, J. L., Campuzano-Jost, P., Froyd, K. D., Liao, J., Hair, J. W., Fenn, M. A., Butler, C. F., Wagner, N. L., Gordon, T. D., Welti, A., Wennberg, P. O., Crounse, J. D., St Clair, J. M., Teng, A. P., Millet, D. B., Schwarz, J. P., Markovic, M. Z., and Perring, A. E.: Sources, seasonality, and trends of southeast US aerosol: an integrated analysis of surface, aircraft, and satellite observations with the GEOS-Chem chemical transport model, Atmos Chem Phys, 15, 10411-10433, 10.5194/acp-15-10411-2015, 2015.

Kroll, J. H., Ng, N. L., Murphy, S. M., Flagan, R. C., and Seinfeld, J. H.: Secondary organic aerosol formation from isoprene photooxidation, Environ Sci Technol, 40, 1869-1877, 10.1021/es0524301, 2006.

Lamarque, J. F., Bond, T. C., Eyring, V., Granier, C., Heil, A., Klimont, Z., Lee, D., Liousse, C., Mieville, A., Owen, B., Schultz, M. G., Shindell, D., Smith, S. J., Stehfest, E., Van Aardenne, J., Cooper, O. R., Kainuma, M., Mahowald, N., McConnell, J. R., Naik, V., Riahi, K., and van Vuuren, D. P.: Historical (1850-2000) gridded anthropogenic and biomass burning emissions of reactive gases and aerosols: methodology and application, Atmos Chem Phys, 10, 7017-7039, 10.5194/acp-10-7017-2010, 2010.

Lamsal, L. N., Krotkov, N. A., Celarier, E. A., Swartz, W. H., Pickering, K. E., Bucsela, E. J., Gleason, J. F., Martin, R. V., Philip, S., Irie, H., Cede, A., Herman, J., Weinheimer, A., Szykman, J. J., and Knepp, T. N.: Evaluation of OMI operational standard NO2 column retrievals using in situ and surface-based NO2 observations, Atmos Chem Phys, 14, 11587-11609, 10.5194/acp-14-11587-2014, 2014.

Lee, A., Goldstein, A. H., Kroll, J. H., Ng, N. L., Varutbangkul, V., Flagan, R. C., Seinfeld, J. H., Gas-phase products and secondary aerosol yields from the photooxidation of 16 different terpenes, J Geosphy Res- Atmos, 111, D17, https://doi.org/10.1029/2006JD007050, 2006.

Lee-Taylor, J., Hodzic, A., Madronich, S., Aumont, B., Camredon, M., and Valorso, R.: Multiday production of condensing organic aerosol mass in urban and forest outflow, Atmos Chem Phys, 15, 595-615, 10.5194/acp-15-595-2015, 2015.

Levelt, P. F., Van den Oord, G. H. J., Dobber, M. R., Malkki, A., Visser, H., de Vries, J., Stammes, P., Lundell, J. O. V., and Saari, H.: The Ozone Monitoring Instrument, Ieee T Geosci Remote, 44, 1093-1101, 10.1109/Tgrs.2006.872333, 2006.

Levy, R. C., Munchak, L. A., Mattoo, S., Patadia, F., Remer, L. A., and Holz, R. E.: Towards a long-term global aerosol optical depth record: applying a consistent aerosol retrieval algorithm to MODIS and VIIRS-observed reflectance, Atmos Meas Tech, 8, 4083-4110, 10.5194/amt-8-4083-2015, 2015.

Liu, X. X., Huey, L. G., Yokelson, R. J., Selimovic, V., Simpson, I. J., Muller, M., Jimenez, J. L., Campuzano-Jost, P., Beyersdorf, A. J., Blake, D. R., Butterfield, Z., Choi, Y., Crounse, J. D., Day, D. A., Diskin, G. S., Dubey, M. K., Fortner, E., Hanisco, T. F., Hu, W. W., King, L. E.,

1117 Kleinman, L., Meinardi, S., Mikoviny, T., Onasch, T. B., Palm, B. B., Peischl, J., Pollack, I. B.,
1118 Ryerson, T. B., Sachse, G. W., Sedlacek, A. J., Shilling, J. E., Springston, S., St Clair, J. M.,
1119 Tanner, D. J., Teng, A. P., Wennberg, P. O., Wisthaler, A., and Wolfe, G. M.: Airborne
1120 measurements of western US wildfire emissions: Comparison with prescribed burning and air
1121 quality implications, J Geophys Res-Atmos, 122, 6108-6129, 10.1002/2016jd026315, 2017.
1122
1123 Malm, W. C., Sisler, J. F., Huffman, D., Eldred, R. A., and Cahill, T. A.: Spatial and Seasonal
1124 Trends in Particle Concentration and Optical Extinction in the United-States, J Geophys Res-
1125 Atmos, 99, 1347-1370, Doi 10.1029/93jd02916, 1994.
1126
1127 Malm, W. C., Schichtel, B. A., Hand, J. L., and Collett, J. L.: Concurrent Temporal and Spatial
1128 Trends in Sulfate and Organic Mass Concentrations Measured in the IMPROVE Monitoring
1129 Program, J Geophys Res-Atmos, 122, 10341-10355, 10.1002/2017jd026865, 2017.
1130
1131 Marais, E. A., Jacob, D. J., Jimenez, J. L., Campuzano-Jost, P., Day, D. A., Hu, W., Krechmer,
1132 J., Zhu, L., Kim, P. S., Miller, C. C., Fisher, J. A., Travis, K., Yu, K., Hanisco, T. F., Wolfe, G.
1133 M., Arkinson, H. L., Pye, H. O. T., Froyd, K. D., Liao, J., and McNeill, V. F.: Aqueous-phase
1134 mechanism for secondary organic aerosol formation from isoprene: application to the southeast
1135 United States and co-benefit of SO2 emission controls, Atmos Chem Phys, 16, 1603-1618,
1136 10.5194/acp-16-1603-2016, 2016.
1137
1138 Marais, E. A., Jacob, D. J., Turner, J. R., and Mickley, L. J.: Evidence of 1991-2013 decrease of
1139 biogenic secondary organic aerosol in response to SO2 emission controls, Environ Res Lett, 12,
1140 ARTN 054018
1141 10.1088/1748-9326/aa69c8, 2017.
1142
1143 McDonald, B. C., de Gouw, J. A., Gilman, J. B., Jathar, S. H., Akherati, A., Cappa, C. D.,
1144 Jimenez, J. L., Lee-Taylor, J., Hayes, P. L., McKeen, S. A., Cui, Y. Y., Kim, S. W., Gentner, D.
1145 R., Isaacman-VanWertz, G., Goldstein, A. H., Harley, R. A., Frost, G. J., Roberts, J. M.,
1146 Ryerson, T. B., and Trainer, M.: Volatile chemical products emerging as largest petrochemical
1147 source of urban organic emissions, Science, 359, 760-764, ARTN aaq0524
1148 10.1126/science.aaq0524, 2018.
1149
1150 Millet, D. B., Jacob, D. J., Boersma, K. F., Fu, T. M., Kurosu, T. P., Chance, K., Heald, C. L.,
1151 and Guenther, A.: Spatial distribution of isoprene emissions from North America derived from
1152 formaldehyde column measurements by the OMI satellite sensor, J Geophys Res-Atmos, 113,
1153 Artn D02307
1154 10.1029/2007jd008950, 2008.
1155
1156 Murphy, D. M., Cziczo, D. J., Froyd, K. D., Hudson, P. K., Matthew, B. M., Middlebrook, A.
1157 M., Peltier, R. E., Sullivan, A., Thomson, D. S., and Weber, R. J.: Single-particle mass
1158 spectrometry of tropospheric aerosol particles, J Geophys Res-Atmos, 111, Artn D23s32
1159 10.1029/2006jd007340, 2006.
1160
1161 Na, K., Kim, Y. P., and Moon, K. C.: Seasonal variation of the C-2-C-9 hydrocarbons
1162 concentrations and compositions emitted from motor vehicles in a Seoul tunnel, Atmos Environ,

36, 1969-1978, Pii S1352-2310(02)00149-8
Doi 10.1016/S1352-2310(02)00149-8, 2002.

Na, K., Moon, K. C., and Kim, Y. P.: Source contribution to aromatic VOC concentration and ozone formation potential in the atmosphere of Seoul, Atmos Environ, 39, 5517-5524, 10.1016/j.atmosenv.2005.06.005, 2005.

NASA OMI $NO_2$ data archive, data product OMI-Aura_L3-OMNO2d, hbps://disc.sci.gsfc.nasa.gov, last accessed: 4 January, 2017.

NASA MODIS AOD data archive, data product MYD04_L2, hbps://ladsweb.nascom.nasa.gov/, last accessed: 20 October, 2019.

Nault, B. A., Campuzano-Jost, P., Day, D. A., Schroder, J. C., Anderson, B., Beyersdorf, A. J., Blake, D. R., Brune, W. H., Choi, Y., Corr, C. A., de Gouw, J. A., Dibb, J., DiGangi, J. P., Diskin, G. S., Fried, A., Huey, L. G., Kim, M. J., Knote, C. J., Lamb, K. D., Lee, T., Park, T., Pusede, S. E., Scheuer, E., Thornhill, K. L., Woo, J.-H., and Jimenez, J. L.: Secondary Organic Aerosol Production from Local Emissions Dominates the Organic Aerosol Budget over Seoul, South Korea, during KORUS-AQ, Atmos. Chem. Phys., 18, 17769-17800, https://doi.org/10.5194/acp-2018-838, 2018.

Ng, N. L., Kroll, J. H., Chan, A. W. H., Chhabra, P. S., Flagan, R. C., and Seinfeld, J. H.: Secondary organic aerosol formation from m-xylene, toluene, and benzene, Atmos Chem Phys, 7, 3909-3922, DOI 10.5194/acp-7-3909-2007, 2007.

Palm, B. B., de Sa, S. S., Day, D. A., Campuzano-Jost, P., Hu, W. W., Seco, R., Sjostedt, S. J., Park, J. H., Guenther, A. B., Kim, S., Brito, J., Wurm, F., Artaxo, P., Thalman, R., Wang, J., Yee, L. D., Wernis, R., Isaacman-VanWertz, G., Goldstein, A. H., Liu, Y. J., Springston, S. R., Souza, R., Newburn, M. K., Alexander, M. L., Martin, S. T., and Jimenez, J. L.: Secondary organic aerosol formation from ambient air in an oxidation flow reactor in central Amazonia, Atmos Chem Phys, 18, 467-493, 10.5194/acp-18-467-2018, 2018.

Pope, C. A., Burnett, R. T., Thun, M. J., Calle, E. E., Krewski, D., Ito, K., and Thurston, G. D.: Lung cancer, cardiopulmonary mortality, and long-term exposure to fine particulate air pollution, Jama-J Am Med Assoc, 287, 1132-1141, DOI 10.1001/jama.287.9.1132, 2002.

Pye, H. O. T., Chan, A. W. H., Barkley, M. P., and Seinfeld, J. H.: Global modeling of organic aerosol: the importance of reactive nitrogen (NOx and NO3), Atmos Chem Phys, 10, 11261-11276, 10.5194/acp-10-11261-2010, 2010.

Pye, H. O. T., Murphy, B. N., Xu, L., Ng, N. L., Carlton, A. G., Guo, H., Weber, R., Vasilakos, P., Appel, K. W., Budisulistiorini, S. H., Surratt, J. D., Nenes, A., Hu, W., Jimenez, J. L., Isaacman-VanWertz, G., Misztal, P. K., and Goldstein, A. H.: On the implications of aerosol liquid water and phase separation for organic aerosol mass, Atmos. Chem. Phys., 17, 343-369, https://doi.org/10.5194/acp-17-343-2017, 2017.

Richter, D., Weibring, P., Walega, J. G., Fried, A., Spuler, S. M., and Taubman, M. S.: Compact highly sensitive multi-species airborne mid-IR spectrometer, Appl Phys B-Lasers O, 119, 119-131, 10.1007/s00340-015-6038-8, 2015.

Ridley, D. A., Heald, C. L., Ridley, K. J., and Kroll, J. H.: Causes and consequences of decreasing atmospheric organic aerosol in the United States, P Natl Acad Sci USA, 115, 290-295, 10.1073/pnas.1700387115, 2018.

Robinson, A. L., Donahue, N. M., Shrivastava, M. K., Weitkamp, E. A., Sage, A. M., Grieshop, A. P., Lane, T. E., Pierce, J. R., and Pandis, S. N.: Rethinking organic aerosols: Semivolatile emissions and photochemical aging, Science, 315, 1259-1262, 10.1126/science.1133061, 2007.

Ryerson, T. B., Andrews, A. E., Angevine, W. M., Bates, T. S., Brock, C. A., Cairns, B., Cohen, R. C., Cooper, O. R., de Gouw, J. A., Fehsenfeld, F. C., Ferrare, R. A., Fischer, M. L., Flagan, R. C., Goldstein, A. H., Hair, J. W., Hardesty, R. M., Hostetler, C. A., Jimenez, J. L., Langford, A. O., McCauley, E., McKeen, S. A., Molina, L. T., Nenes, A., Oltmans, S. J., Parrish, D. D., Pederson, J. R., Pierce, R. B., Prather, K., Quinn, P. K., Seinfeld, J. H., Senff, C. J., Sorooshian, A., Stutz, J., Surratt, J. D., Trainer, M., Volkamer, R., Williams, E. J., and Wofsy, S. C.: The 2010 California Research at the Nexus of Air Quality and Climate Change (CalNex) field study, J Geophys Res-Atmos, 118, 5830-5866, 10.1002/jgrd.50331, 2013.

Ryerson, T. B., Trainer, M., Holloway, J. S., Parrish, D. D., Huey, L. G., Sueper, D. T., Frost, G. J., Donnelly, S. G., Schauffler, S., Atlas, E. L., Kuster, W. C., Goldan, P. D., Hubler, G., Meagher, J. F., and Fehsenfeld, F. C.: Observations of ozone formation in power plant plumes and implications for ozone control strategies, Science, 292, 719-723, DOI 10.1126/science.1058113, 2001.

Seco, R., Karl, T., Guenther, A., Hosman, K. P., Pallardy, S. G., Gu, L. H., Geron, C., Harley, P., and Kim, S.: Ecosystem-scale volatile organic compound fluxes during an extreme drought in a broadleaf temperate forest of the Missouri Ozarks (central USA), Global Change Biol, 21, 3657-3674, 10.1111/gcb.12980, 2015.

Schroder, J.C, P. Campuzano-Jost, D.A. Day, V. Shah, K. Larson, J.M. Sommers, A.P. Sullivan, T. Campos, J.M. Reeves, A. Hills, R. S. Hornbrook, N.J. Blake, E. Scheuer, H. Guo, D.L. Fibiger, E.E. McDuffie, P.L. Hayes, R.J. Weber, J.E. Dibb, E.C. Apel, L. Jaeglé, S.S. Brown, J.A. Thornton, J.L. Jimenez. Sources and Secondary Production of Organic Aerosols in the Northeastern US during WINTER. J. Geophys. Res.-Atmos., 123, https://doi.org/10.1029/2018JD028475, 2018.

Shrivastava, M., Cappa, C. D., Fan, J. W., Goldstein, A. H., Guenther, A. B., Jimenez, J. L., Kuang, C., Laskin, A., Martin, S. T., Ng, N. L., Petaja, T., Pierce, J. R., Rasch, P. J., Roldin, P., Seinfeld, J. H., Shilling, J., Smith, J. N., Thornton, J. A., Volkamer, R., Wang, J., Worsnop, D. R., Zaveri, R. A., Zelenyuk, A., and Zhang, Q.: Recent advances in understanding secondary organic aerosol: Implications for global climate forcing, Rev Geophys, 55, 509-559, 10.1002/2016rg000540, 2017.

Solomon, P. A., Crumpler, D., Flanagan, J. B., Jayanty, R. K. M., Rickman, E. E., and McDade,

C. E.: US National PM2.5 Chemical Speciation Monitoring Networks-CSN and IMPROVE: Description of networks, J Air Waste Manage, 64, 1410-1438, 10.1080/10962247.2014.956904, 2014.

Stocker, T.F., D. Qin, G.-K. Plattner, M. Tignor, S.K. Allen, J. Boschung, A. Nauels, Y. Xia, V. Bex and P.M. Midgley (eds.), IPCC, 2013: *Climate Change 2013: The Physical Science Basis. Contribution of Working Group I to the Fifth Assessment Report of the Intergovernmental Panel on Climate Change*. Cambridge University Press, Cambridge, United Kingdom and New York, NY, USA, 1535 pp, doi:10.1017/CBO9781107415324.

Taylor, K. E., and Penner, J. E.: Response of the Climate System to Atmospheric Aerosols and Greenhouse Gases, Nature, 369, 734-737, DOI 10.1038/369734a0, 1994.

Tong, D. Q., Lamsal, L., Pan, L., Ding, C., Kim, H., Lee, P., Chai, T. F., Pickering, K. E., and Stajner, I.: Long-term NOx trends over large cities in the United States during the great recession: Comparison of satellite retrievals, ground observations, and emission inventories, Atmos Environ, 107, 70-84, 10.1016/j.atmosenv.2015.01.035, 2015.

Toon, O. B., Maring, H., Dibb, J., Ferrare, R., Jacob, D. J., Jensen, E. J., Luo, Z. J., Mace, G. G., Pan, L. L., Pfister, L., Rosenlof, K. H., Redemann, J., Reid, J. S., Singh, H. B., Thompson, A. M., Yokelson, R., Minnis, P., Chen, G., Jucks, K. W., and Pszenny, A.: Planning, implementation, and scientific goals of the Studies of Emissions and Atmospheric Composition, Clouds and Climate Coupling by Regional Surveys (SEAC(4)RS) field mission, J Geophys Res-Atmos, 121, 4967-5009, 10.1002/2015jd024297, 2016.

Torres, O., Tanskanen, A., Veihelmann, B., Ahn, C., Braak, R., Bhartia, P. K., Veefkind, P., and Levelt, P.: Aerosols and surface UV products from Ozone Monitoring Instrument observations: An overview, J Geophys Res-Atmos, 112, Artn D24s47 10.1029/2007jd008809, 2007.

Travis, K. R., Jacob, D. J., Fisher, J. A., Kim, P. S., Marais, E. A., Zhu, L., Yu, K., Miller, C. C., Yantosca, R. M., Sulprizio, M. P., Thompson, A. M., Wennberg, P. O., Crounse, J. D., St Clair, J. M., Cohen, R. C., Laughner, J. L., Dibb, J. E., Hall, S. R., Ullmann, K., Wolfe, G. M., Pollack, I. B., Peischl, J., Neuman, J. A., and Zhou, X. L.: Why do models overestimate surface ozone in the Southeast United States?, Atmos Chem Phys, 16, 13561-13577, 10.5194/acp-16-13561-2016, 2016.

Tsigaridis, K., Daskalakis, N., Kanakidou, M., Adams, P. J., Artaxo, P., Bahadur, R., Balkanski, Y., Bauer, S. E., Bellouin, N., Benedetti, A., Bergman, T., Berntsen, T. K., Beukes, J. P., Bian, H., Carslaw, K. S., Chin, M., Curci, G., Diehl, T., Easter, R. C., Ghan, S. J., Gong, S. L., Hodzic, A., Hoyle, C. R., Iversen, T., Jathar, S., Jimenez, J. L., Kaiser, J. W., Kirkevag, A., Koch, D., Kokkola, H., Lee, Y. H., Lin, G., Liu, X., Luo, G., Ma, X., Mann, G. W., Mihalopoulos, N., Morcrette, J. J., Muller, J. F., Myhre, G., Myriokefalitakis, S., Ng, N. L., O'Donnell, D., Penner, J. E., Pozzoli, L., Pringle, K. J., Russell, L. M., Schulz, M., Sciare, J., Seland, O., Shindell, D. T., Sillman, S., Skeie, R. B., Spracklen, D., Stavrakou, T., Steenrod, S. D., Takemura, T., Tiitta, P.,

1301 Tilmes, S., Tost, H., van Noije, T., van Zyl, P. G., von Salzen, K., Yu, F., Wang, Z., Wang, Z.,
1302 Zaveri, R. A., Zhang, H., Zhang, K., Zhang, Q., and Zhang, X.: The AeroCom evaluation and
1303 intercomparison of organic aerosol in global models, Atmos Chem Phys, 14, 10845-10895,
1304 10.5194/acp-14-10845-2014, 2014.
1305
1306 Veefkind, J. P., Boersma, K. F., Wang, J., Kurosu, T. P., Krotkov, N., Chance, K., and Levelt, P.
1307 F.: Global satellite analysis of the relation between aerosols and short-lived trace gases, Atmos
1308 Chem Phys, 11, 1255-1267, 10.5194/acp-11-1255-2011, 2011.
1309
1310 Wagner, N. L., Brock, C. A., Angevine, W. M., Beyersdorf, A., Campuzano-Jost, P., Day, D., de
1311 Gouw, J. A., Diskin, G. S., Gordon, T. D., Graus, M. G., Holloway, J. S., Huey, G., Jimenez, J.
1312 L., Lack, D. A., Liao, J., Liu, X., Markovic, M. Z., Middlebrook, A. M., Mikoviny, T., Peischl,
1313 J., Perring, A. E., Richardson, M. S., Ryerson, T. B., Schwarz, J. P., Warneke, C., Welti, A.,
1314 Wisthaler, A., Ziemba, L. D., and Murphy, D. M.: In situ vertical profiles of aerosol extinction,
1315 mass, and composition over the southeast United States during SENEX and SEAC(4)RS:
1316 observations of a modest aerosol enhancement aloft, Atmos Chem Phys, 15, 7085-7102,
1317 10.5194/acp-15-7085-2015, 2015.
1318
1319 Walgraeve, C., Demeestere, K., Dewulf, J., Zimmermann, R., and Van Langenhove, H.:
1320 Oxygenated polycyclic aromatic hydrocarbons in atmospheric particulate matter: Molecular
1321 characterization and occurrence, Atmos Environ, 44, 1831-1846,
1322 10.1016/j.atmosenv.2009.12.004, 2010.
1323
1324 Warneke, C., de Gouw, J. A., Stohl, A., Cooper, O. R., Goldan, P. D., Kuster, W. C., Holloway,
1325 J. S., Williams, E. J., Lerner, B. M., McKeen, S. A., Trainer, M., Fehsenfeld, F. C., Atlas, E. L.,
1326 Donnelly, S. G., Stroud, V., Lueb, A., and Kato, S.: Biomass burning and anthropogenic sources
1327 of CO over New England in the summer 2004, J Geophys Res-Atmos, 111, Artn D23s15
1328 10.1029/2005jd006878, 2006.
1329
1330 Warneke, C., Veres, P., Holloway, J. S., Stutz, J., Tsai, C., Alvarez, S., Rappenglueck, B.,
1331 Fehsenfeld, F. C., Graus, M., Gilman, J. B., and de Gouw, J. A.: Airborne formaldehyde
1332 measurements using PTR-MS: calibration, humidity dependence, inter-comparison and initial
1333 results, Atmos Meas Tech, 4, 2345-2358, 10.5194/amt-4-2345-2011, 2011.
1334
1335 Weibring, P., Richter, D., Fried, A., Walega, J. G., and Dyroff, C.: Ultra-high-precision mid-IR
1336 spectrometer II: system description and spectroscopic performance, Appl Phys B-Lasers O, 85,
1337 207-218, 10.1007/s00340-006-2300-4, 2006.
1338
1339 Wisthaler A., Hansel A., Dickerson R. R., Crutzen P. J.: Organic trace gas measurements
1340 by PTR-MS during INDOEX 1999, J Geosphys Res-Atmos, 107(D19), 8024, 2002.
1341
1342 Wolfe, G. M., Kaiser, J., Hanisco, T. F., Keutsch, F. N., de Gouw, J. A., Gilman, J. B., Graus,
1343 M., Hatch, C. D., Holloway, J., Horowitz, L. W., Lee, B. H., Lerner, B. M., Lopez-Hilifiker, F.,
1344 Mao, J., Marvin, M. R., Peischl, J., Pollack, I. B., Roberts, J. M., Ryerson, T. B., Thornton, J. A.,
1345 Veres, P. R., and Warneke, C.: Formaldehyde production from isoprene oxidation across NOx
1346 regimes, Atmos Chem Phys, 16, 2597-2610, 10.5194/acp-16-2597-2016, 2016.

Worton, D.R., J.D. Surratt, B.W. Lafranchi, A.W.H. Chan, Y. Zhao, R. Weber, J. Park, J.B. Gilman, J. de Gouw, C. Park, G. Schade, M. Beaver, J. StClair, J. Crounse, P. Wennberg, G. Wolfe, S. Harrold, J. Thornton, D. K. Farmer, K.S. Docherty, Mi.J. Cubison, J.L. Jimenez, A. Frossard, L. Russell, K. Kristensen, M. Glasius, J. Mao, X. Ren, W.H. Brune, E. Browne, S. Pusede, R. Cohen, J.H. Seinfeld and A.H. Goldstein. Observational Insights into Aerosol Formation from Isoprene. Environmental Science & Technology, 47, 11403-11413, doi:10.1021/es4011064, 2013.

Xu, L., Middlebrook, A. M., Liao, J., de Gouw, J. A., Guo, H. Y., Weber, R. J., Nenes, A., Lopez-Hilfiker, F. D., Lee, B. H., Thornton, J. A., Brock, C. A., Neuman, J. A., Nowak, J. B., Pollack, I. B., Welti, A., Graus, M., Warneke, C., and Ng, N. L.: Enhanced formation of isoprene-derived organic aerosol in sulfur-rich power plant plumes during Southeast Nexus, J Geophys Res-Atmos, 121, 11137-11153, 10.1002/2016jd025156, 2016.

Xu, L., Suresh, S., Guo, H., Weber, R. J., and Ng, N. L.: Aerosol characterization over the southeastern United States using high-resolution aerosol mass spectrometry: spatial and seasonal variation of aerosol composition and sources with a focus on organic nitrates, Atmos Chem Phys, 15, 7307-7336, 10.5194/acp-15-7307-2015, 2015.

Yu, K. R., Jacob, D. J., Fisher, J. A., Kim, P. S., Marais, E. A., Miller, C. C., Travis, K. R., Zhu, L., Yantosca, R. M., Sulprizio, M. P., Cohen, R. C., Dibb, J. E., Fried, A., Mikoviny, T., Ryerson, T. B., Wennberg, P. O., and Wisthaler, A.: Sensitivity to grid resolution in the ability of a chemical transport model to simulate observed oxidant chemistry under high-isoprene conditions, Atmos Chem Phys, 16, 4369-4378, 10.5194/acp-16-4369-2016, 2016.

Zhang, H. F., Yee, L. D., Lee, B. H., Curtis, M. P., Worton, D. R., Isaacman-VanWertz, G., Offenberg, J. H., Lewandowski, M., Kleindienst, T. E., Beaver, M. R., Holder, A. L., Lonneman, W. A., Docherty, K. S., Jaoui, M., Pye, H. O. T., Hu, W. W., Day, D. A., Campuzano-Jost, P., Jimenez, J. L., Guo, H. Y., Weber, R. J., de Gouw, J., Koss, A. R., Edgerton, E. S., Brune, W., Mohr, C., Lopez-Hilfiker, F. D., Lutz, A., Kreisberg, N. M., Spielman, S. R., Hering, S. V., Wilson, K. R., Thornton, J. A., and Goldstein, A. H.: Monoterpenes are the largest source of summertime organic aerosol in the southeastern United States, P Natl Acad Sci USA, 115, 2038-2043, 10.1073/pnas.1717513115, 2018.

Zhu, L., Jacob, D. J., Keutsch, F. N., Mickley, L. J., Scheffe, R., Strum, M., Abad, G. G., Chance, K., Yang, K., Rappengluck, B., Millet, D. B., Baasandorj, M., Jaegle, L., and Shah, V.: Formaldehyde (HCHO) As a Hazardous Air Pollutant: Mapping Surface Air Concentrations from Satellite and Inferring Cancer Risks in the United States, Environ Sci Technol, 51, 5650-5657, 10.1021/acs.est.7b01356, 2017.

Zhu, L., Jacob, D. J., Kim, P. S., Fisher, J. A., Yu, K., Travis, K. R., Mickley, L. J., Yantosca, R. M., Sulprizio, M. P., De Smedt, I., Abad, G. G., Chance, K., Li, C., Ferrare, R., Fried, A., Hair, J. W., Hanisco, T. F., Richter, D., Scarino, A. J., Walega, J., Weibring, P., and Wolfe, G. M.: Observing atmospheric formaldehyde (HCHO) from space: validation and intercomparison of six retrievals from four satellites (OMI, GOME2A, GOME2B, OMPS) with SEAC(4)RS aircraft

observations over the southeast US, Atmos Chem Phys, 16, 13477-13490, 10.5194/acp-16-13477-2016, 2016.

Ziemann, P.J., and Atkinson, R. Kinetics, products, and mechanisms of secondary organic aerosol formation. Chem. Soc. Rev., 41, 6582-6605, doi: 10.1039/C2CS35122F, 2012.

Tables

Table 1. Linear regression parameters for OA vs. HCHO at low altitudes (<1 km)

| | US (SEAC$^4$RS) | US (DC3) | US (CalNex) | South Korea (KORUS-AQ) | Wild Fires (SEAC$^4$RS) | Agricultural Fires (SEAC$^4$RS) | SEAC$^4$RS Low $NO_2$ and Isoprene | SEAC$^4$RS high $NO_2$ and Isoprene |
|---|---|---|---|---|---|---|---|---|
| **In situ measurements OA v.s. HCHO** | | | | | | | | |
| Slope [a] | 1.93±0.07 | 1.30± 0.10 | 1.34±0.02 | 2.75±0.05 | 25.08±0.30 | 3.22±0.37 | 2.39±0.09 | 1.45±0.19 |
| Slope [b] ($\times10^{-11}$) | 9.61± 0.34 | 6.49± 0.49 | 6.66±0.09 | 13.7 1 ± 0.25 | 125. 05 ± 1.49 | 16.04 ± 1.85 | 11.9±043 | 7.25±0.96 |
| Intercept[c] | 0.34±032 | 1.10±0.30 | -0.90±0.06 | 1.36±0.22 | −6.85±2.80 | 10.41±5.82 | −1.14±0.37 | 1.14±1.22 |
| Correlation coefficient r | 0.59 | 0.76 | 0.88 | 0.70 | 0.97 | 0.85 | 0.64 | 0.45 |
| Number of points (1 min avg) | 1506 | 134 | 1772 | 3425 | 515 | 32 | 1138 | 226 |
| **GEOS- Chem model sampled along the flight track OA v.s. HCHO** | | | | | | | | |
| Slope[a] | 1.25±0.03 | | | 1.39±0.05 | 0.48±0.05 | | | |
| Slope ($\times10^{-11}$) | 6.21± 0.14 | | | 6.95± 0.23 | 2.37± 0.22 | | | |
| Intercept | −1.32 ±0.11 | | | 1.88 ± 0.07 | 0.12±0.03 | | | |
| Correlation Coefficient r | 0.76 | | | 0.43 | 0.53 | | | |

[a] The unit of the slope is g $g^{-1}$.
[b] The unit of the slope is pg $molec^{-1}$.
[c] The unit of the intercept is μg $m^{-3}$.
The uncertainties are one standard deviation.

Table 2. Cases to estimate OA surface concentrations, based on the choice of slope and intercept from a linear regression relationship between OA and HCHO data found in Table 1.

| | |
|---|---|
| LUMP-SUM[a] | Using non-BB SEAC$^4$RS relationship to represent all continental US |
| ISOP-NOx[b] | Using $NO_2$ and isoprene dependent non-BB SEAC$^4$RS relationship for all continental US |
| URBAN | Using the CalNex LA Basin relationship for large urban cites and the non-biomass burning SEAC$^4$RS relationship for other US regions |
| COMBINE[b] | Using the CalNex LA Basin relationship for large urban cites and the $NO_2$ and isoprene dependent non-BB SEAC$^4$RS relationship for other US regions |

[a]SEAC$^4$RS was chosen to represent all continental US because it had the largest horizontal and vertical coverage.

[b] In cases ISOP-$NO_x$ and COMBINE, when the product of $NO_2$ column (Sect. 2.3) and surface isoprene emission rate (Sect. 2.4) was above threshold of $5\times10^{27}$ molec $cm^{-2}$ atom C $cm^{-2}$ $s^{-1}$, the slope and intercept from SEAC$^4$RS high isoprene and $NO_2$ conditions were used. When the $NO_2$ column−isoprene emission

product was below that threshold, the slope and intercept from SEAC$^4$RS low isoprene and $NO_2$ conditions were used. Threshold of "Isoprene × $NO_2$" was determined by its mean value over SE US (83° - 96° W and 32° - 35°N). Large urban cities were categorized with high $NO_2$ vertical columns (>4 ×$10^{15}$ molec $cm^{-2}$) (Tong et al., 2015) based on the satellite $NO_2$ levels over LA. Isoprene emissions instead of concentrations were used because global models use isoprene emission inventory to simulate isoprene concentrations and isoprene emission inventory is easier to access. Since isoprene has a short-lifetime of up to a few hours (Guenther et al., 2006), the emissions have a similar spatiotemporal distribution as the concentrations.

Figures

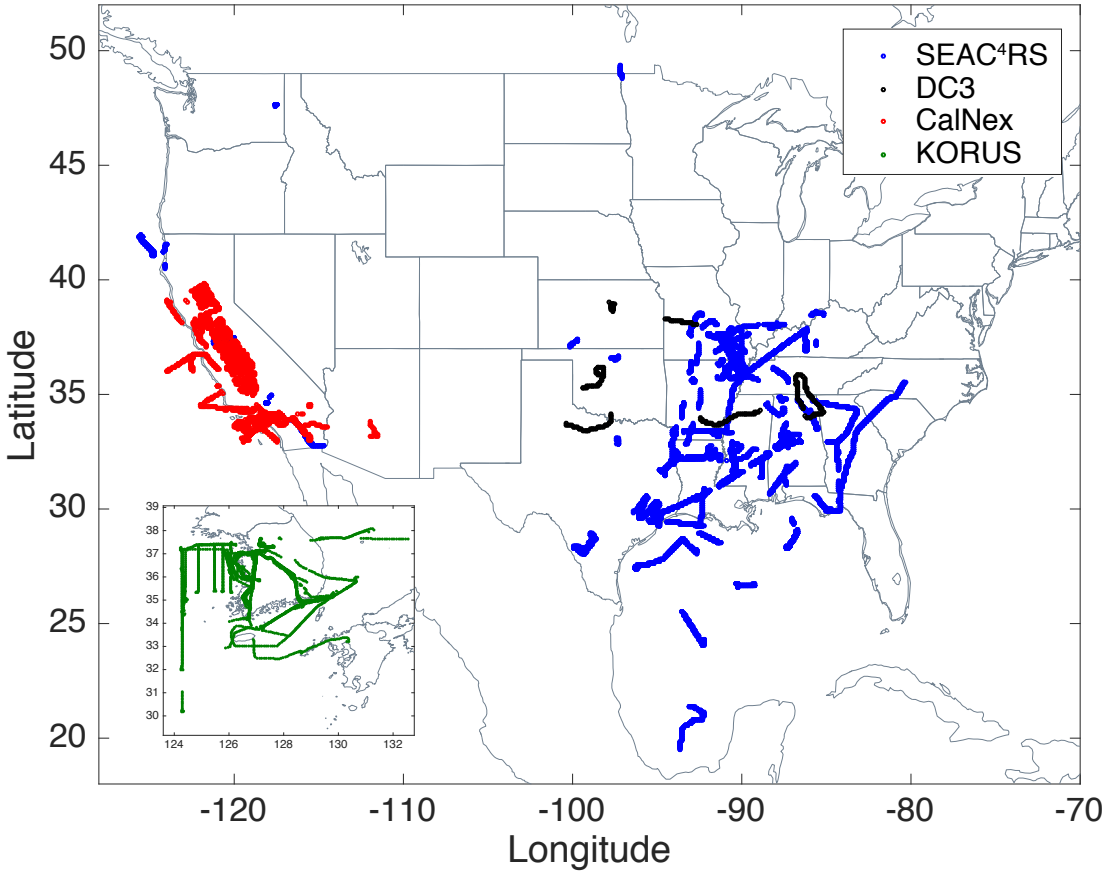


Figure 1. Flight tracks of airborne field campaigns SEAC$^4$RS (blue), DC3 (black), CalNex (red) and KORUS-AQ (green) with altitudes (< 1 km), of which in situ OA and HCHO measurements were used.

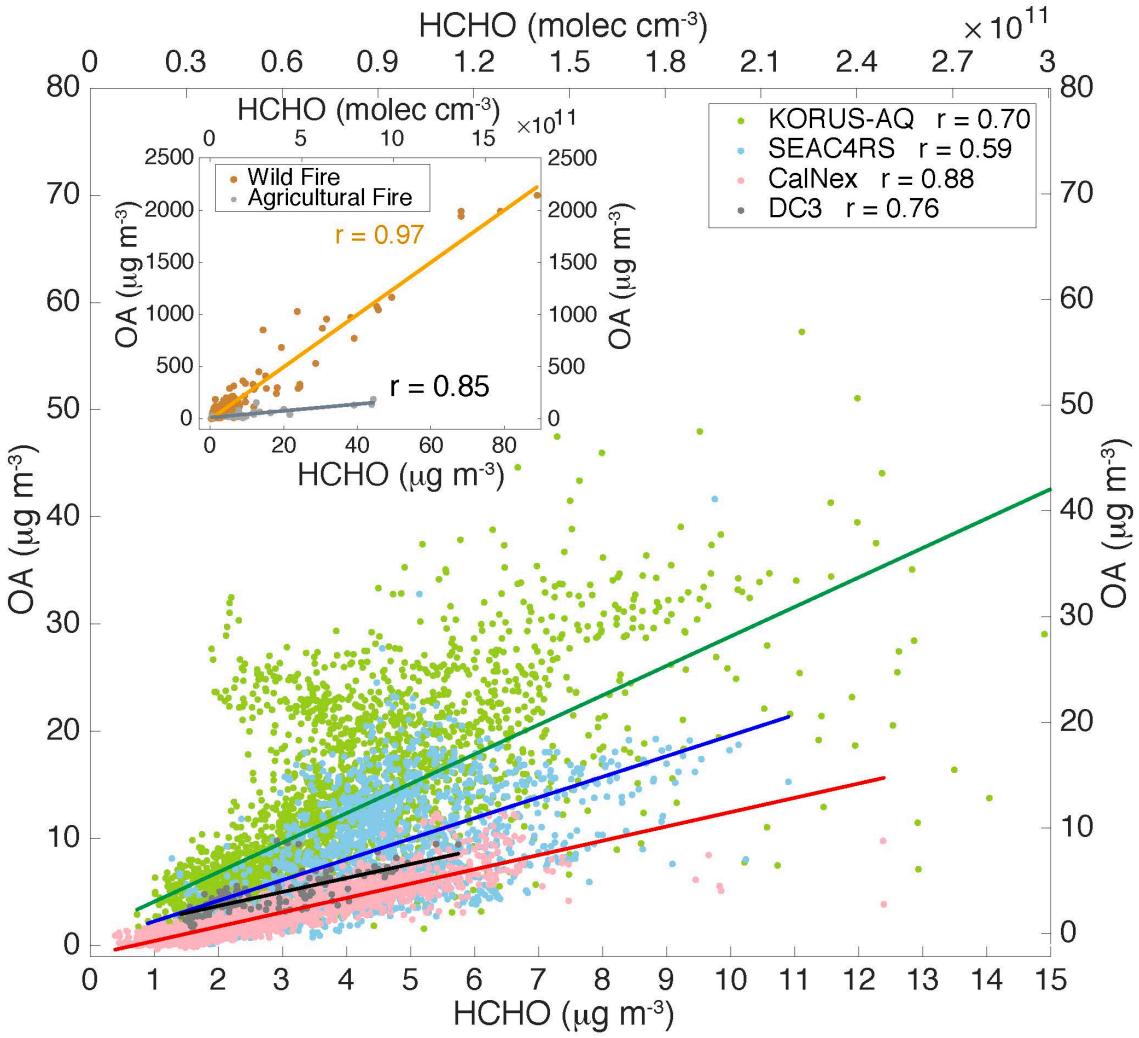


Figure 2

Scatter plots of in situ OA (µg $m^{-3}$) vs. HCHO (µg $m^{-3}$ or molec $cm^{-3}$) from SEAC$^4$RS (excluding biomass burning) (blue), DC3 (dark grey), CalNex (pink), and KORUS-AQ (green) low altitude (< 1 km) data. Inset shows wildfire (brown), and agricultural fire (grey) SEAC$^4$RS data. SEAC$^4$RS biomass burning cases are defined as acetonitrile > 200 pptv. The linear regression fits are shown as the darker lines and correlation coefficients are provided.

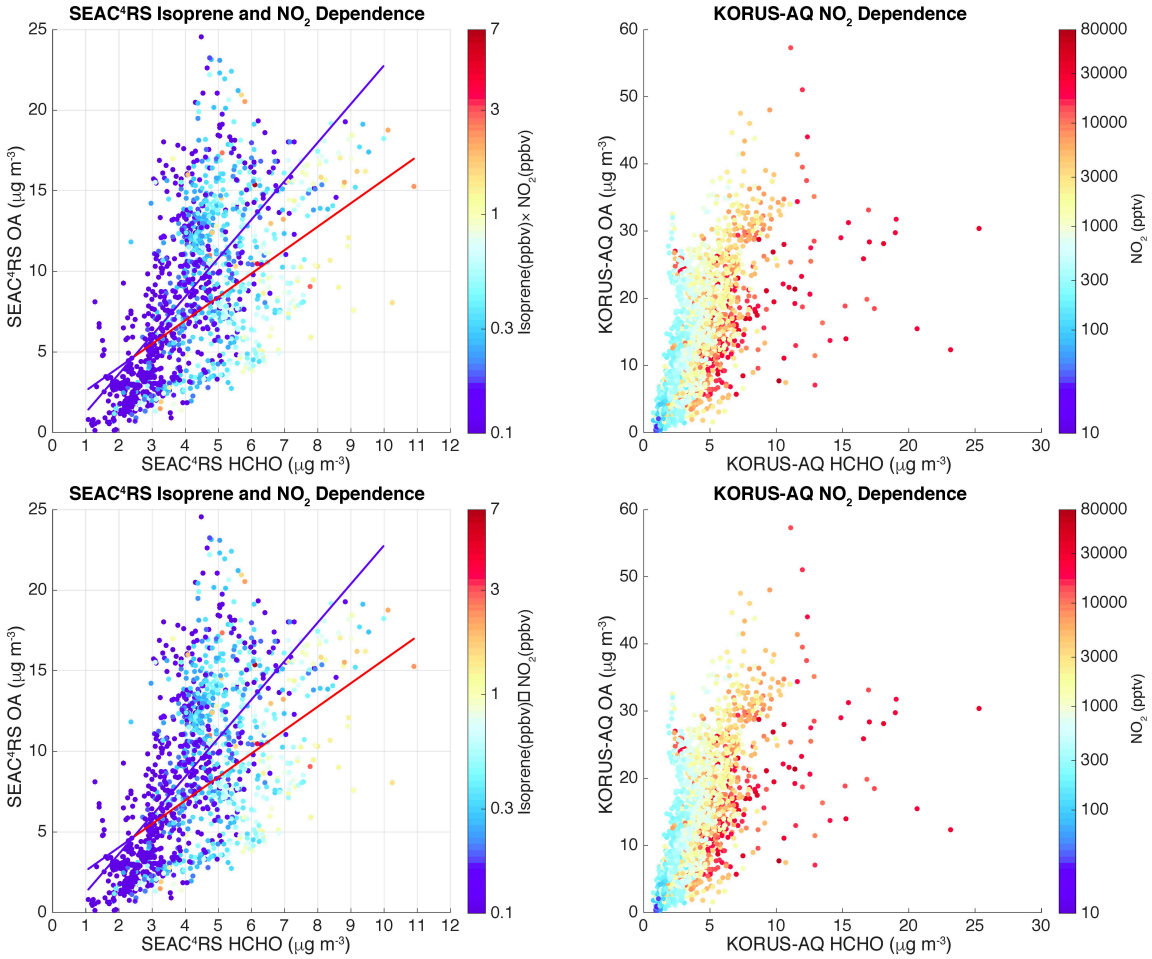


Figure 3. (a) A scatter plot of OA vs. HCHO for SEAC$^4$RS non-biomass burning low altitude data color-coded with the product of $NO_2$ and isoprene in log scale. The red and blue lines are the linear regression fits of high (> 0.5) and low (<0.5) product of $NO_2$ (ppbv) and isoprene (ppbv), respectively. (b) A scatter plot of OA vs. HCHO for KORUS-AQ data color-coded by log($NO_2$).

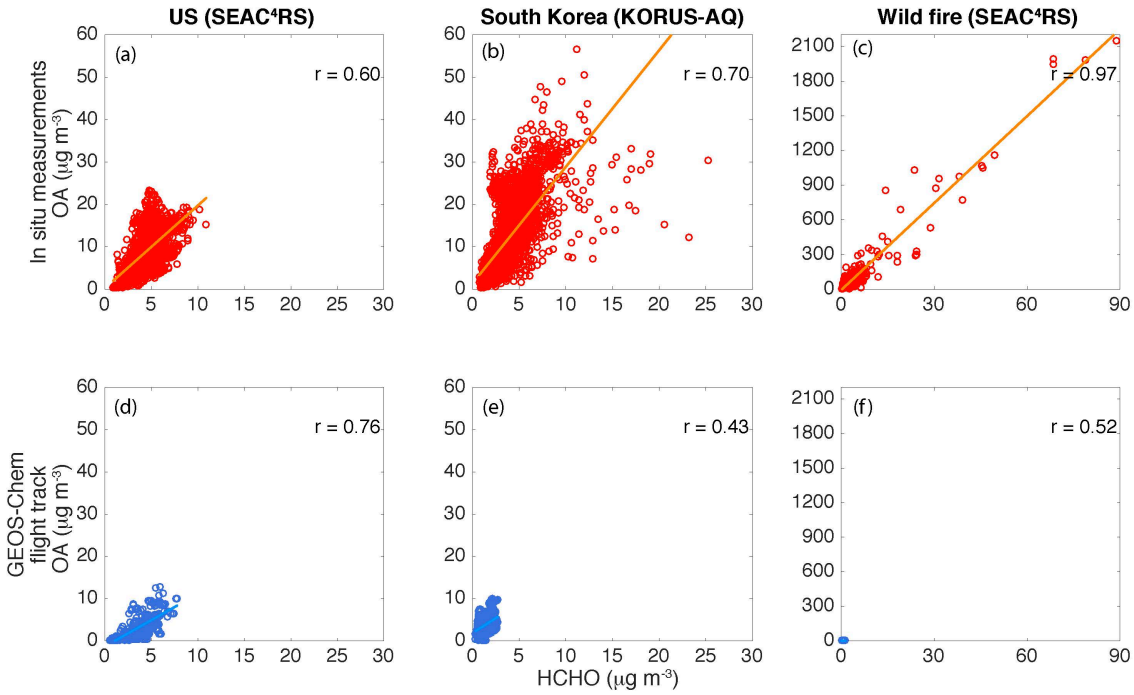


Figure 4 Scatter plots of OA vs. HCHO for US (SEAC$^4$RS altitude < 1 km non-biomass burning), South Korea (KORUS-AQ altitude < 1 km) and wildfire (SEAC$^4$RS) from in situ measurements (a, b, c) and GEOS-Chem outputs sampled along the flight tracks (d,e,f).

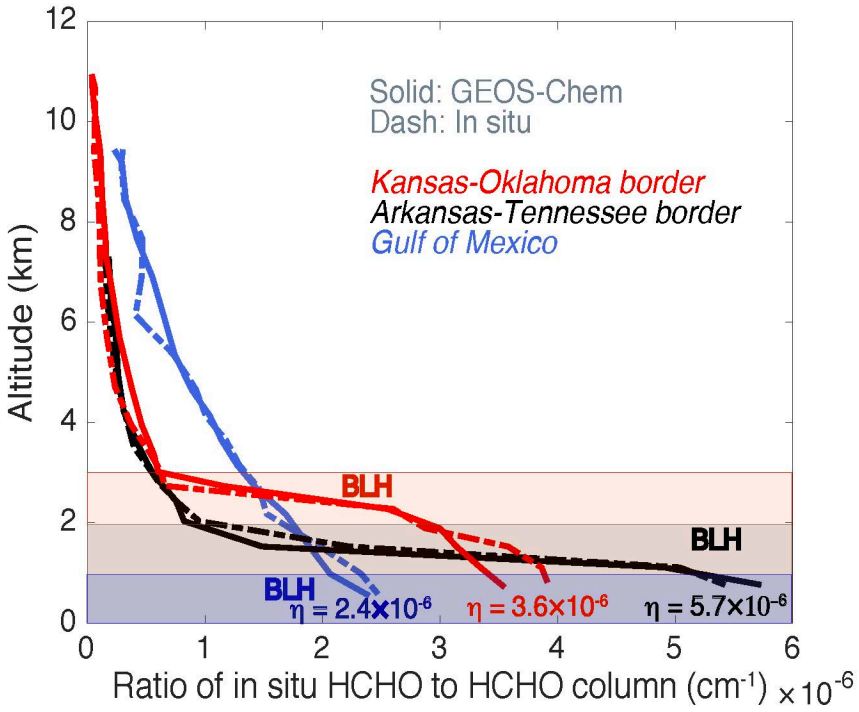


Figure 5. Three typical vertical profiles of the ratio of in situ HCHO concentrations (molec $cm^{-3}$) to integrated HCHO column from SEAC$^4$RS flight track. These three profiles were located at Kansas-Oklahoma border (red), Arkansas-Tennessee border (black), and Gulf of Mexico (blue). Solid curves were from GEOS-Chem results and the dashed were from ISAF measurements. HCHO columns were integrated HCHO concentrations of these vertical profiles extrapolated from 0 to 10 km, assuming the HCHO below and above the measured HCHO vertical profiles were the same as the HCHO at the lowest and highest altitudes sampled, respectively. The boundary layer heights (BLH) of these three profiles are plotted by the shaded areas.

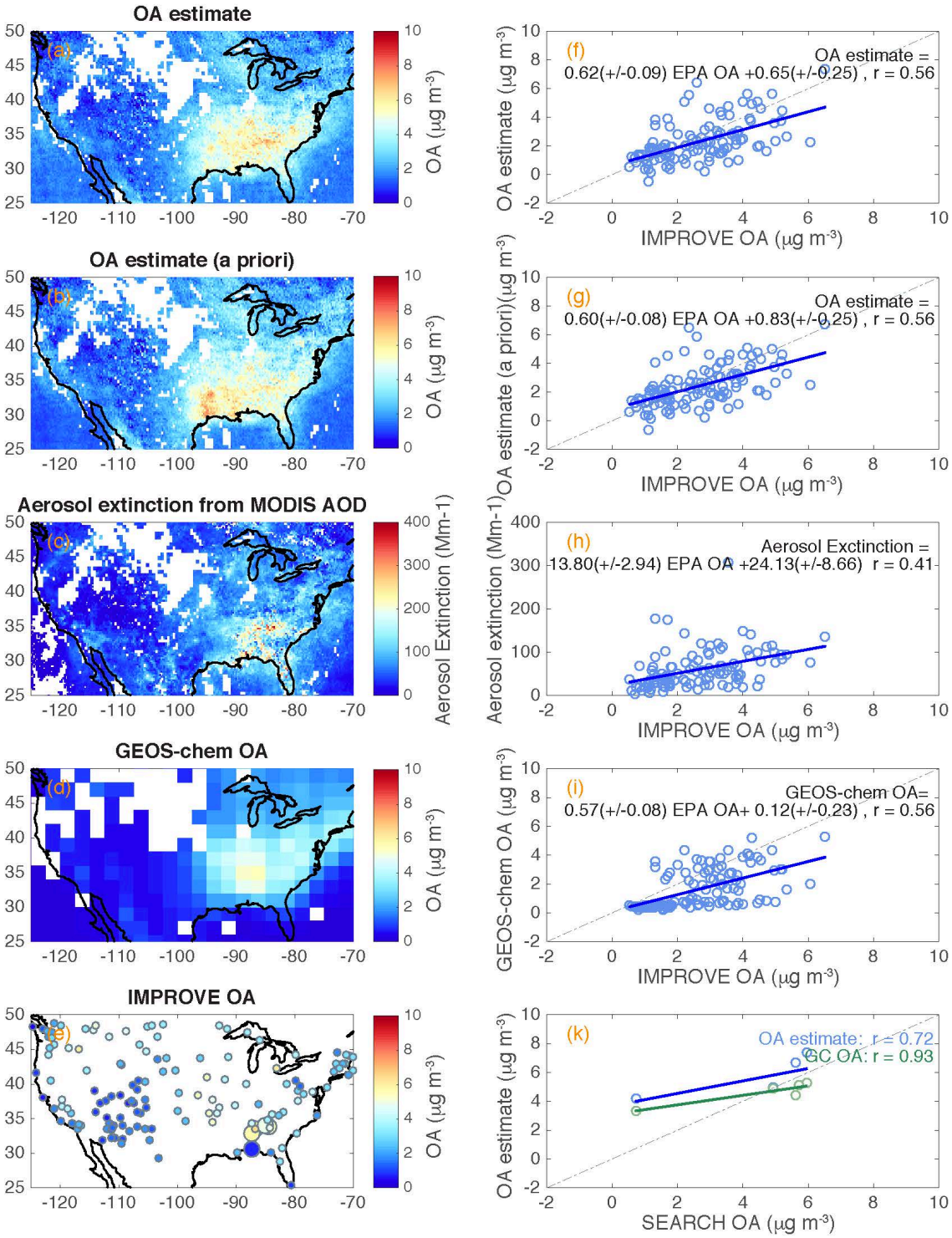


Figure 6. (a) The maps of (a) surface OA estimate (Case 1) with $\eta$ from GEOS-Chem v9-02, (b) surface OA estimate (Case 1) with $\eta$ from a priori profiles, (c) surface aerosol extinction derived from MODIS AOD, (d) GEOS-Chem simulated surface OA, and (e) EPA IMPROVE (small dots) and SEARCH (large dots) network ground sites color coded with OA concentrations for August 2013. The scatter plots of (f,g) surface OA estimate, (h) surface aerosol extinction derived from MODIS AOD, and (i) surface GEOS-Chem

OA vs. EPA IMPROVE network ground sites OA. IMPROVE sites OA were corrected for evaporation. (k) The scatter plots of surface OA estimate and GEOS-Chem OA vs. SEARCH network ground sites OA for August 2013. GEOS-Chem OA and OA estimate did not have good correlations with SEARCH OA for other years (SI). For the scatter plots, linear regressions are shown (blue and green lines) and regression equations and correlation coefficients for the scatter plots are listed. The dashed lines in the scatter plots indicate the 1 : 1 line. Biomass burning data (UV aerosol index > 1.6) were excluded in all panels.

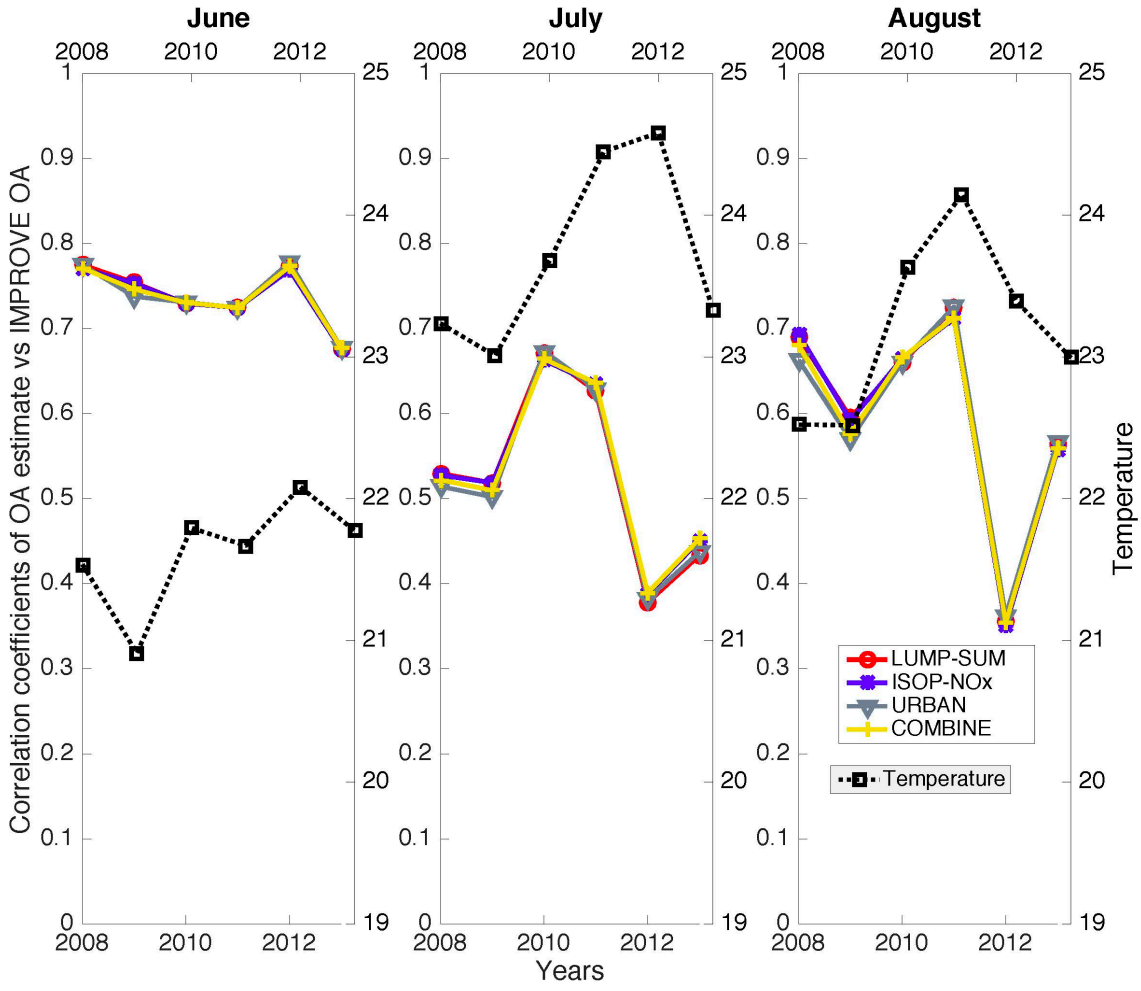


Figure 7. The correlation coefficients of the linear regression between the OA estimate from 4 case (red, blue, gray, and yellow) vs. EPA-corrected OA from 2008 – 2013 for June, July, and August. The monthly average ambient temperature is in black.